

PASTA: Controllable Part-Aware Shape Generation with Autoregressive Transformers

SONGLIN LI, Stanford University, USA
 DESPOINA PASCHALIDOU, Stanford University, USA
 LEONIDAS GUIBAS, Stanford University, USA

The increased demand for tools that automate the 3D content creation process led to tremendous progress in deep generative models that can generate diverse 3D objects of high fidelity. In this paper, we present PASTA, an autoregressive transformer architecture for generating high quality 3D shapes. PASTA comprises two main components: An autoregressive transformer that generates objects as a sequence of cuboidal primitives and a blending network, implemented with a transformer decoder that composes the sequences of cuboids and synthesizes high quality meshes for each object. Our model is trained in two stages: First we train our autoregressive generative model using only annotated cuboidal parts as supervision and next, we train our blending network using explicit 3D supervision, in the form of watertight meshes. Evaluations on various ShapeNet objects showcase the ability of our model to perform shape generation from diverse inputs e.g. from scratch, from a partial object, from text and images, as well size-guided generation, by explicitly conditioning on a bounding box that defines the object’s boundaries. Moreover, as our model considers the underlying part-based structure of a 3D object, we are able to select a specific part and produce shapes with meaningful variations of this part. As evidenced by our experiments, our model generates 3D shapes that are both more realistic and diverse than existing part-based and non part-based methods, while at the same time is simpler to implement and train.

CCS Concepts: • **Computing methodologies** → **Shape modeling**.

Additional Key Words and Phrases: Generative Models, Shape Editing, Autoregressive Transformers, Controllable Part-Aware Shape Synthesis

1 INTRODUCTION

The ability to generate realistic and diverse 3D shapes has the potential to significantly accommodate the workflow of artists and content creators and potentially enable new levels of creativity through "generative art" [Bailey 2020]. The tremendous progress in generative modelling and implicit-based representations gave rise to several works [Chan et al. 2022, 2021; Gao et al. 2022; Gu et al. 2022; Schwarz et al. 2020] that generate objects with high realism in terms of geometric details and texture. Nevertheless, as these pipelines represent objects holistically, i.e. without taking into consideration the underlying part-based structure of each object, they only support few interactive applications that typically require deep technical knowledge of each model. However, shape editing and manipulation involves controlling what parts of the object need to be changed. To enable this level of control, an active area of research proposes to consider the decomposition of shapes into parts [Deprelle et al. 2019; Gadelha et al. 2020; Hao et al. 2020; Hertz et al. 2022; Li et al. 2021; Mo et al. 2019a, 2020; Wu et al. 2020].

Existing part-based generative models, represent 3D shapes as a collection of simple shapes parametrized with cuboids [Mo et al.

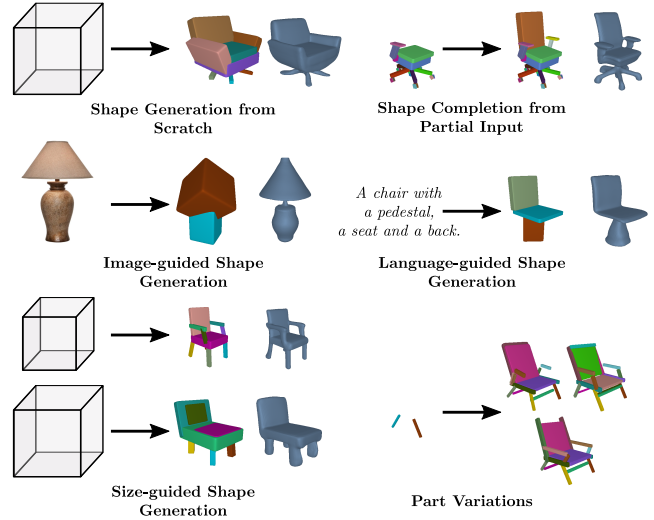


Fig. 1. **Controllable Part-Aware 3D Shape Generation.** We propose a novel autoregressive architecture that can be used to perform several editing tasks, such as generating novel shapes from scratch, conditioned on a bounding box defining the object’s boundaries, completing a 3D shape from a partial input, a text, an image or bounding boxes of different sizes, as well as generating plausible variations for specific parts of the object.

2019a, 2020; Wu et al. 2020; Zou et al. 2017], spheres [Hao et al. 2020], implicit fields [Hertz et al. 2022; Wu et al. 2020] or more general handles [Gadelha et al. 2020; Liu et al. 2021], and seek to synthesize new shapes in accordance to their underlying structural understanding of the object. For example, among the first to explore structure-based generative models were [Li et al. 2017; Mo et al. 2019a] that utilized an autoencoder for generating structured shapes. Despite their impressive capabilities on shape generation and interpolation neither can perform shape completion from a partial input or generate plausible part variations. Similarly, while [Wu et al. 2020; Zou et al. 2017] can generate 3D shapes as a sequences of parts, they need to train a separate model for different editing tasks, namely the same model cannot perform both shape generation and shape completion, which makes their approach impractical.

To address these limitations, we devise PASTA, a novel part-aware generative model for 3D shapes. PASTA comprises two main components: An autoregressive transformer encoder that generates shapes as unordered sets of parts and a blending network, implemented as a transformer decoder that combines the part sequences and produces high-quality meshes. Each component of our architecture is trained independently. In particular, we optimize our autoregressive transformer to maximize the log-likelihood of all part arrangements in the dataset. Our supervision comes in the form of part labels

Authors’ addresses: Songlin Li, Stanford University, 353 Jane Stanford Way, Stanford, CA, 94305, USA, svli97@stanford.edu; Despoina Paschalidou, Stanford University, 353 Jane Stanford Way, Stanford, CA, 94305, USA, paschal@stanford.edu; Leonidas Guibas, Stanford University, 353 Jane Stanford Way, Stanford, CA, 94305, USA, guibas@stanford.edu.

and 3D cuboids that specify the per-part size and pose. Unlike existing autoregressive pipelines [Paschalidou et al. 2021a; Tulsiani and Gupta 2021] that are trained using teacher forcing, we train PASTA using scheduled sampling [Bengio et al. 2015; Mihaylova and Martins 2019] and showcase that it significantly improves the generation performance of our model. To train our blending network, we consider 3D supervision in the form of watertight meshes and optimize it to reconstruct 3D shapes as implicit occupancy fields [Mescheder et al. 2019]. We evaluate the performance of our model on several PartNet [Mo et al. 2019b] objects and demonstrate that our model can produce more realistic and diverse 3D objects in comparison to both part-based [Paschalidou et al. 2021a; Wu et al. 2020] and non part-based methods [Chen and Zhang 2019]. Furthermore, we showcase that our model can generate meaningful part arrangements conditioned on versatile user input (Fig. 1) including but not limited to text and images.

In summary we make the following **contributions**: We propose the first part-aware generative model using an autoregressive transformer architecture. Our experiments on various PartNet objects [Mo et al. 2019b] demonstrate that our model generates more diverse and plausible 3D shapes in comparison to part-based [Paschalidou et al. 2021a; Wu et al. 2020] and non part-based methods [Chen and Zhang 2019]. Furthermore, our simple, yet effective architecture allows training a single model capable of performing several editing operations, such as generating new objects from scratch, generating part variations or completing partial shapes.

2 RELATED WORK

3D Representations Learning-based approaches for 3D reconstruction employ a neural network that learns a function from the input to a mesh [Groueix et al. 2018; Kanazawa et al. 2018; Liao et al. 2018; Pan et al. 2019; Wang et al. 2018b; Yang et al. 2019], a pointcloud [Achlioptas et al. 2018; Fan et al. 2017; Jiang et al. 2018; Qi et al. 2017; Thomas et al. 2019; Yang et al. 2019], a voxel grid [Brock et al. 2016; Choy et al. 2016; Gadelha et al. 2017; Rezende et al. 2016; Riegler et al. 2017; Stutz and Geiger 2018; Xie et al. 2019] or an implicit surface [Chen and Zhang 2019; Mescheder et al. 2019; Michalkiewicz et al. 2019; Park et al. 2019; Saito et al. 2019; Xu et al. 2019]. Unlike explicit representations that discretize the output space, using voxels, points or mesh vertices, implicit representations represent shapes in the weights of a neural network that learns a mapping between a query point and a context vector to a signed distance value [Atzmon and Lipman 2020; Gropp et al. 2020; Michalkiewicz et al. 2019; Park et al. 2019; Takikawa et al. 2021] or a binary occupancy value [Chen and Zhang 2019; Mescheder et al. 2019]. As these methods require 3D supervision, several works propose combining them with surface [Niemeyer et al. 2020; Yariv et al. 2020] or volumetric [Mildenhall et al. 2020] rendering to learn the 3D object geometry and texture directly from images. In this work, we introduce a part-aware generative model that parametrizes shapes as an occupancy field [Mescheder et al. 2019].

Primitive-based Representations Shape abstraction techniques represent shapes using semantically consistent part arrangements and seek to recover the 3D geometry using simple shapes such as cuboids [Dubrovina et al. 2019; Li et al. 2017; Mo et al. 2019a;

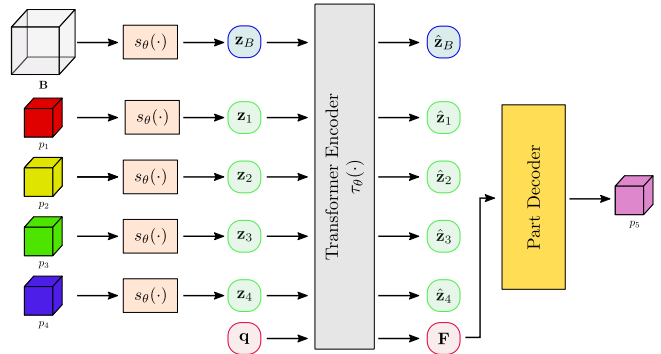


Fig. 2. **Object Generator.** Given a sequence of N parts and a bounding box B defining the object boundaries, the *part encoder* $s_{\theta}(\cdot)$ maps each part p_j and the bounding box to an embedding vector. The bounding box’s embedding vector z_B , the per-part embeddings $\{z_j\}_{j=1}^N$ and a learnable embedding vector q are passed to the *transformer decoder* that predicts a feature vector F used to predict the attributes of the next part in the sequence. The *part decoder* takes F and autoregressively predicts the attribute distributions that are used to sample the attributes for the next part.

Niu et al. 2018; Tulsiani et al. 2017; Zou et al. 2017], superquadrics [Paschalidou et al. 2019, 2020], convex solids [Chen et al. 2020b; Deng et al. 2020; Gadelha et al. 2020], spheres [Hao et al. 2020] and 3D Gaussians [Genova et al. 2019]. In recent work, [Paschalidou et al. 2021b] proposed to represent objects as a family of homeomorphic mappings, parametrized with an Invertible Neural Network (INN) [Dinh et al. 2015]. Likewise, [Genova et al. 2020] suggested to represent 3D objects using a structured set of implicit functions [Genova et al. 2019]. Another line of research employs primitives to recover the 3D geometry using CSG trees [Sharma et al. 2018] or shape programs [Ellis et al. 2018; Liu et al. 2019; Tian et al. 2019]. Very recently [Yao et al. 2021, 2022], explored learning primitive-based representations only from images. Unlike these works that focus on recovering the object geometry as a collection of parts, we introduce a part-aware generative model that synthesizes novel objects as a set of cuboidal primitives.

3D Generative Models Generative Adversarial Networks (GANs) [Goodfellow et al. 2014] have demonstrated impressive capabilities on several image synthesis [Brock et al. 2019; Choi et al. 2018; Huang et al. 2018; Karras et al. 2019, 2020] and editing [Alharbi and Wonka 2020; Choi et al. 2018; Isola et al. 2017; Ling et al. 2021; Shen et al. 2020; Wang and Ponce 2021; Wang et al. 2018a; Zhu et al. 2017] tasks. However, adapting them to 3D content creation is non-trivial as they ignore the 3D nature of the world and hence, lack an understanding of the object’s underlying geometry. To address this, 3D-aware GANs proposed to incorporate 3D representations such as voxel grids [Henzler et al. 2019; Nguyen-Phuoc et al. 2019, 2020] in generative settings or combine them with differentiable renderers [Liao et al. 2020; Zhang et al. 2021]. As an alternative, several works explored generating 3D shapes as octrees [Ibing et al. 2021], pointclouds [Achlioptas et al. 2018; Cai et al. 2020; Li et al. 2021; Luo and Hu 2021; Yang et al. 2019; Zhou et al. 2021], meshes [Luo et al. 2021; Nash et al. 2020; Pavllo et al. 2021, 2020] and implicit functions [Chen et al. 2020b; Mescheder et al. 2019]. While these methods yield realistic geometries, they do not consider the part-based object

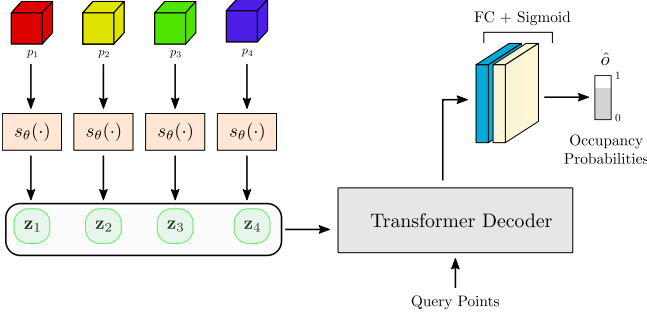


Fig. 3. **Blending Network.** Given a sequence of N parts, the *part encoder* maps them into embedding vectors $\{z_j\}_{j=1}^N$. We pass the per-part embedding vectors and a set of 3D query points \mathcal{X} to the *transformer decoder* that predicts the occupancy probabilities for the query points.

structure. In contrast, we propose a part-aware generative model that generates shapes as an unordered set of cuboids, which are then combined and synthesize a high quality implicit shape.

Part-based Generative Models Our work falls into the category of part-based generative models. Zou et al. [Zou et al. 2017] was among the first to introduce a generative recurrent model, parametrized with LSTMs [Hochreiter and Schmidhuber 1997] in combination with a Mixture Density Network (MDN) to synthesize novel objects as a set of cuboids. Concurrently, Li et al. [Li et al. 2017] proposed to represent shapes using a symmetry hierarchy, which defines how parts are recursively grouped by symmetry and assembled by connectivity [Wang et al. 2011]. In particular, they utilize an RNN and generate objects as bounding box layouts, which are then filled with voxelized parts. Likewise, StructureNet [Mo et al. 2019a] utilizes a VAE [Kingma and Ba 2015] and generates novel shapes as n -ary graphs, where every node in the graph is associated with a bounding box. Note that while [Mo et al. 2019a] can generate plausible new shapes, perform shape and part interpolations, their model cannot be utilized for completion from unconstrained inputs, e.g. a partial object. Furthermore, to perform shape editing, their model requires additional optimization steps in order to find a new shape in the latent space that satisfies a specific edit. Concurrently, [Mo et al. 2020], explored learning a latent space of structured shape differences, using pairs of structured shapes demonstrating a specific edit. Closely related to our work is PQ-NET [Wu et al. 2020] that generates shapes autoregressively using an RNN autoencoder. The RNN encoder takes a 3D shape segmented into parts and extracts per-part features, which are then fed to the decoder that sequentially predicts parts that reconstruct the input shape. To be able to generate new shapes, they train a latent GAN [Achlioptas et al. 2018] on the latent space of the autoencoder. Moreover, to perform different editing tasks, they need to train different variants of their model. Instead, our formulation allows applying a single model trained for object completion on a variety of tasks. Furthermore, instead of using an RNN, we employ an autoregressive transformer that synthesizes objects as a sequence of cuboids, which are passed to our blending network to produce the final high-quality shape.

Autoregressive Transformers for Content Creation Transformer-based architectures [Vaswani et al. 2017] have been extensively

utilized for various autoregressive tasks ranging from machine translation [Ott et al. 2018; Shaw et al. 2018] to image [Chen et al. 2020a; Esser et al. 2021; Katharopoulos et al. 2020; Parmar et al. 2018; Tulsiani and Gupta 2021] and music [Dhariwal et al. 2020] generation, as well as shape completion [Mittal et al. 2022; Yu et al. 2021] and indoor scene synthesis [Paschalidou et al. 2021a; Wang et al. 2020]. Similar to ATISS [Paschalidou et al. 2021a], that is an autoregressive transformer for scene synthesis, we pose object synthesis as an autoregressive prediction problem and generate objects as a sequence of cuboids. However, unlike ATISS that is trained with teacher forcing, we train our model using scheduled sampling [Bengio et al. 2015; Mihaylova and Martins 2019] and showcase that it improves the generation capabilities of our model.

3 METHOD

PASTA is a part-aware generative model for synthesizing 3D shapes. Our model comprises two main components that are trained independently: An *object generator* that sequentially generates objects as unordered sequences of labelled parts, where each part is parametrized using a 3D cuboidal primitive (Sec. 3.1), and a *blending network* that composes part sequences in a meaningful way and synthesizes high quality implicit shapes. The *object generator* is an autoregressive model trained to maximize the log-likelihood of all possible part arrangements in the dataset. We use part-level supervision in the form of part labels and 3D cuboids that define the size and the pose of each part (Sec. 3.2). The *blending network* is an occupancy network [Mescheder et al. 2019], implemented with a transformer decoder that takes a sequence of cuboids and a query 3D point and predicts whether this point is inside or outside the surface boundaries (Sec. 3.3). To train the blending network, we assume explicit 3D supervision in the form of a watertight mesh.

3.1 Object Parametrization

We define each object $\mathcal{S} = \{\mathcal{P}, \mathbf{B}\}$ using a collection of N parts, $\mathcal{P} = \{p_1, \dots, p_N\}$, and a 3D bounding box \mathbf{B} that specifies the object’s boundaries. Each part is represented with a 3D labelled cuboid and is parametrized using four values describing its label, size, translation and rotation, $p_j = \{c_j, s_j, t_j, o_j\}$. To model the label of each part, i.e. the back or the arm of a chair, we use a categorical distribution defined over the total number of part labels in the dataset, whereas for the rest of the attributes we use a mixture of logistic distributions [Salimans et al. 2017; van den Oord et al. 2016]. In our setup, the rotation $o_j \in \mathbb{R}^6$ is the 6D representation [Zhou et al. 2019] of the 3D cuboid that contains the part. Likewise, the translation $t_j \in \mathbb{R}^3$ is the center of the 3D cuboid containing the part and the size $s_j \in \mathbb{R}^3$ is its width, height and depth. Similarly, the bounding box \mathbf{B} is defined using 12 parameters: three for its size along each axis, three for the translation, which is the center of the box and six for the rotation, which is a 6D representation.

Similar to ATISS [Paschalidou et al. 2021a], we predict the components of p_j autoregressively, namely part label first, followed by translation, rotation and size. Hence, the probability of generating the j -th part, conditioned on the previous parts and box \mathbf{B} becomes

$$p_\theta(p_j | p_{<j}, \mathbf{B}) = p_\theta^c(c_j | p_{<j}, \mathbf{B}) p_\theta^t(t_j | c_j, p_{<j}, \mathbf{B}) p_\theta^o(o_j | c_j, t_j, p_{<j}, \mathbf{B}) p_\theta^s(s_j | c_j, t_j, o_j, p_{<j}, \mathbf{B}), \quad (1)$$

where p_θ^c , p_θ^t , p_θ^o and p_θ^s are the probabilities for the respective attributes. Assuming a fixed ordering wrt. the part attributes is reasonable, as we want our model to consider the part label before predicting its pose and size. To compute the likelihood of generating an object \mathcal{S} , we estimate the likelihood of autoregressively generating its parts \mathcal{P} using any order, as [Paschalidou et al. 2021a] demonstrated that not having a fixed ordering can be beneficial. Hence, the likelihood of generating an object \mathcal{S} conditioned on a bounding box \mathbf{B} is

$$p_\theta(\mathcal{S}|\mathbf{B}) = \sum_{\hat{\mathcal{P}} \in \pi(\mathcal{P})} \prod_{j \in \hat{\mathcal{P}}} p_\theta(p_j | p_{<j}, \mathbf{B}), \quad (2)$$

where $\pi(\cdot)$ is a permutation function that computes the set of permutations of all object parts and $\hat{\mathcal{P}}$ denotes an ordered part sequence.

3.2 Object Generator

The input to our *object generator* is a set of objects in the form of 3D labelled cuboids and their corresponding bounding boxes. We implement our generator using an autoregressive transformer architecture similar to ATISS. The transformer model takes as input a sequence of embedding vectors that represent the conditioning sequence and generates the features \mathbf{F} that will be used to predict the attributes of the next part. We map the per-part attributes to embedding vectors using a *part encoder* and the features \mathbf{F} to part attributes using a *part decoder*. Our model is illustrated in Fig. 2.

The part encoder network $s_\theta(\cdot)$ takes the attributes for each part $p_j = \{c_j, s_j, t_j, o_j\}$ and maps them to an embedding vector z_j

$$z_j = s_\theta(\lambda(c_j); \gamma(s_j); \gamma(t_j); \gamma(o_j)), \quad (3)$$

where $\lambda(\cdot)$ is a learnable embedding, $\gamma(\cdot)$ is a positional encoding layer [Vaswani et al. 2017] that is applied separately on each attribute’s dimension and $[\cdot; \cdot]$ denotes concatenation. To predict an embedding vector z_B for \mathbf{B} , we pass its attributes to $s_\theta(\cdot)$.

Similar to ATISS [Paschalidou et al. 2021a], we implement our transformer encoder $\tau_\theta(\cdot)$ as a multi-head attention transformer without positional encoding [Vaswani et al. 2017], as we want to model objects as unordered sets of parts. Our transformer encoder takes as input $\{z_j\}_{j=1}^N$ the N embeddings for all parts in the sequence, z_B the embedding for the bounding box and a learnable embedding vector \mathbf{q} , which is used to predict the feature vector \mathbf{F} that will be used to generate the next part in the sequence. More formally,

$$\mathbf{F} = \tau_\theta(z_B, \{z_j\}_{j=1}^N, \mathbf{q}). \quad (4)$$

The last component of the object generator is the part decoder that takes as input the feature vector \mathbf{F} and autoregressively predicts the attributes of the next part to be generated. For the part label, we define a function $c_\theta(\cdot)$, implemented using a linear projection layer, that takes \mathbf{F} and predicts the per-part label probability. We predict the size, translation and rotation in two-stages. First, we cluster the values of each attribute from the training set into 20 clusters using K-Means. Subsequently, we predict a cluster for each attribute, which is then used to predict the specific values. More formally, for the translation, we learn $t_\theta^{\text{coarse}}(\cdot)$ that predicts the per-cluster probability from \mathbf{F} using a linear projection layer and $t_\theta^{\text{fine}}(\cdot)$ that predicts the $7 \times K$ parameters that define the mixture of logistics

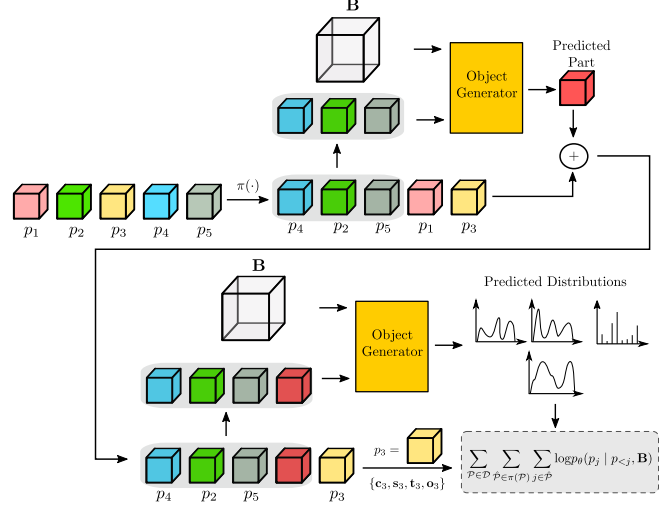


Fig. 4. **Scheduled Sampling.** Given an object with N parts, we first randomly permute them and keep the first M parts (here $M = 3$). We pass them to the object generator that predicts the next part to be generated (red cube). The newly generated cuboid is appended to the initial sequence with the M objects and passed once again to the object generator, that predicts the next part to be generated. Our loss function from (5) is computed between the new part and the $M + 2$ part in the permuted sequence (yellow cube).

distribution for the translation. Specifically, we have K parameters for the mixing coefficients and $6 \times K$ for the means and variances. In a similar manner, we define $o_\theta^{\text{coarse}}(\cdot)$ and $o_\theta^{\text{fine}}(\cdot)$ to predict the $13 \times K$ parameters that define the mixture of logistics distribution for the rotation and $s_\theta^{\text{coarse}}(\cdot)$ and $s_\theta^{\text{fine}}(\cdot)$ that predict the $7 \times K$ parameters that define the mixture of logistic distribution for the size. To predict the part attributes in an autoregressive manner, we condition the prediction of each attribute to the values of the previously predicted ones. In practice, $t_\theta^{\text{coarse}}(\cdot)$, $t_\theta^{\text{fine}}(\cdot)$, $o_\theta^{\text{coarse}}(\cdot)$, $o_\theta^{\text{fine}}(\cdot)$, $s_\theta^{\text{coarse}}(\cdot)$ and $s_\theta^{\text{fine}}(\cdot)$ take as input \mathbf{F} concatenated with the previously predicted attributes embedded by $\lambda(\cdot)$ and $\gamma(\cdot)$ from (3).

3.3 Blending Network

The input to the *blending network* is a sequence of labelled cuboids and a set of 3D query points \mathcal{X} , for which we want to predict their occupancy probabilities, namely whether they lie inside or outside the surface boundaries. In detail, our blending network consists of two main components: (i) a *part-encoder* that maps the part attributes into an embedding vector, which is implemented as discussed in Sec. 3.2 and (ii) a transformer decoder without self-attention that takes the part embeddings and the query points and predicts whether they are inside or outside the surface boundary (see Fig. 3). The transformer comprises only cross attention layers and MLPs, thus, each query 3D point attends to the per-part embeddings using cross attention, without attending to the other points. The transformer output is passed to a linear layer followed by a sigmoid non-linearity to get an occupancy probability for each query point. We follow common practice and before passing the query points to the decoder we map them to a higher dimensional space using positional encoding [Vaswani et al. 2017].

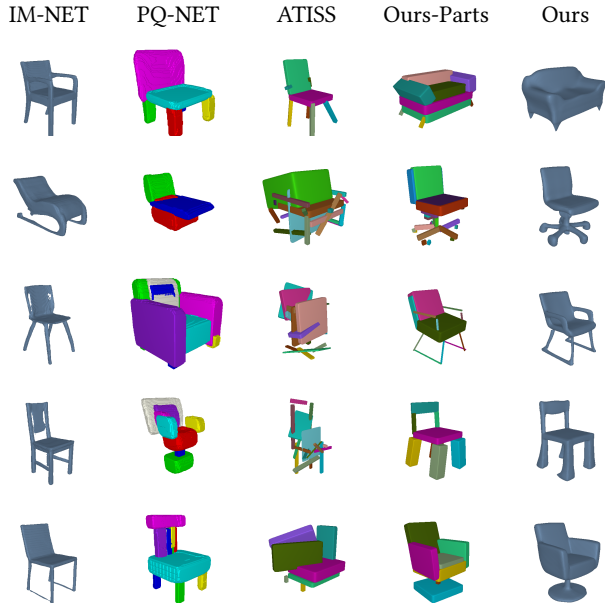


Fig. 5. **Shape Generation Results on Chairs.** We show randomly generated chairs using our model, ATISS, PQ-NET and IM-NET.

| Method | Representation | MMD-CD (\downarrow) | | | | COV-CD ($\%, \uparrow$) | | | |
|------------|----------------|-------------------------|-------------|-------------|-------------|---------------------------|--------------|--------------|--------------|
| | | Chair | Table | Lamp | All | Chair | Table | Lamp | All |
| IM-Net | Implicit | 3.49 | 2.65 | 4.07 | 4.74 | 55.76 | 54.71 | 82.66 | 38.25 |
| PQ-Net | Implicit Parts | 4.49 | 3.94 | 3.73 | 4.82 | 48.93 | 46.44 | 77.56 | 40.41 |
| ATISS | Cuboids | 5.03 | 4.27 | 4.14 | 6.09 | 48.27 | 39.18 | 91.56 | 35.03 |
| Ours-Parts | Cuboids | 3.71 | 3.23 | 4.07 | 3.82 | 57.32 | 57.14 | 81.87 | 51.01 |
| Ours | Implicit | 3.21 | 2.53 | 2.93 | 3.24 | 57.73 | 56.80 | 88.88 | 50.89 |

Table 1. **Shape Generation.** We perform category-specific training (3rd-5th and 7th-9th columns) and joint training on multiple object categories (6th and 10th columns) and report the MMD-CD (\downarrow) and the COV-CD (\uparrow) between generated and real shapes from the test set.

3.4 Training and Inference

Unlike prior autoregressive models [Paschalidou et al. 2021a; Ritchie et al. 2019] that are trained with teacher forced embeddings, we train PASTA using scheduled sampling [Bengio et al. 2015]. The key idea is that during training we feed our model with a mix of the teacher forced embeddings and the actual model’s predictions from the previous generation step. In particular, we choose an object from the dataset and apply the permutation function $\pi(\cdot)$ on its elements. Next, we randomly select the first M objects and pass them to the object generator that is used to predict the next part. The newly generated part is appended to the initial sequence of M parts and passed once again to the object generator to predict the attribute distribution of the next part. Our model is trained to maximize the likelihood of the $M + 2$ object in the permuted sequence. A pictorial representation of our scheduled sampling is provided in Fig. 4. We follow common practice and during training, we train with both scheduled sampling and teacher forcing.

To train the object generator we follow [Paschalidou et al. 2021a] and maximize the likelihood of generating all possible part sequences in the dataset \mathcal{D} in all possible permutations, as follows

$$\mathcal{L}(\theta) = \sum_{\mathcal{P} \in \mathcal{D}} \sum_{\hat{\mathcal{P}} \in \pi(\mathcal{P})} \sum_{j \in \hat{\mathcal{P}}} \log p_{\theta}(p_j | p_{<j}, \mathbf{B}). \quad (5)$$

For the mixture of logistic distributions, we use the discretized mixture of logistics loss as defined in [van den Oord et al. 2016]. To train the blending network, we assume 3D supervision in the form of a watertight mesh, which we use to generate a set of occupancy pairs $\mathcal{X} = \{\{\mathbf{x}_i, o_i\}\}_{i=1}^V$, namely a set of 3D points \mathbf{x}_i and their occupancy labels o_i , denoting whether \mathbf{x}_i lies inside or outside the object. We train the blending network using a classification loss between the predicted and the target occupancies. Note that the blending network is trained using ground-truth part sequences.

During inference, we start from a bounding box \mathbf{B} and autoregressively sample the attribute values from the predicted distributions for the next part to be generated. Once a new part is generated, it is used in the next generation step until the *end symbol* is predicted. To indicate the end of sequence, we augment the part labels with an additional category, which we refer to as *end symbol*. Once a complete sequence of parts is generated, we pass it to the blending network that combines them into a single implicit shape.

3.5 Conditional Generation

Here, we discuss how PASTA can be used to perform language- and image-guided generation. Instead of conditioning the generation only on the bounding box \mathbf{B} , we now condition also on a textual description of the shape to be generated. In particular, we utilize the pre-trained CLIP [Radford et al. 2021] model to extract text embeddings and pass them to the transformer encoder as an additional input. Note that during training the pre-trained CLIP text encoder remains frozen, namely is not optimized with the rest of our network. Once we train PASTA with text embeddings from CLIP, we can use it, without any re-training, also for image-guided generation. This is possible because the CLIP model has a joint latent space for text and images. While, in our experiments, we only demonstrate language- and image-guided generations, our model can be extended to other types of conditioning such as depth maps or pointclouds etc. by utilizing an appropriate encoder that generates embeddings from the input.

4 EXPERIMENTAL EVALUATION

In this section, we provide an extensive evaluation of our method comparing it to relevant baselines. Additional results and implementation details are provided in the supplementary.

Datasets We report results on three PartNet [Mo et al. 2019b] categories: *Chair*, *Table* and *Lamp*, which contain 4489, 5705, and 1554 shapes respectively. For the *Chair* category, there are 47 different types of parts, while for the *Lamp* and the *Table* we have 32 and 43 respectively. We train our model and our part-based baselines using the part annotations and train/test splits from PartNet. Moreover, for our model, we use the object bounding boxes specified in PartNet.

Baselines In our evaluation, we include PQ-NET [Wu et al. 2020] that is a generative model that generates 3D shapes using an RNN

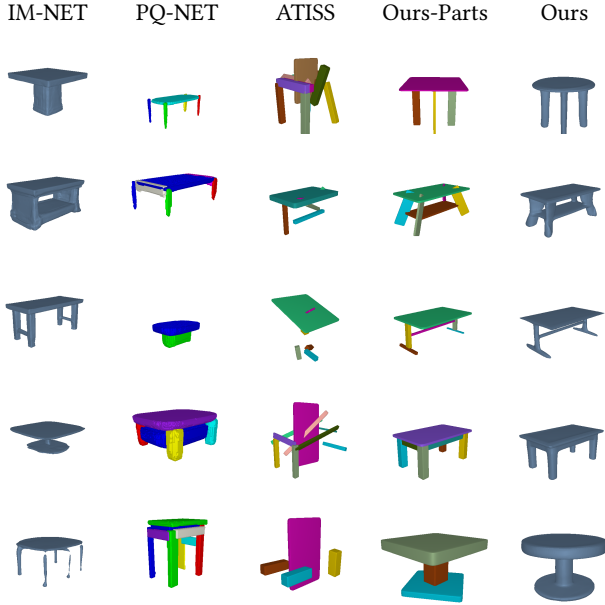


Fig. 6. **Shape Generation Results on Tables.** We show randomly generated tables using our model, ATISS, PQ-NET and IM-NET.

autoencoder, ATISS [Paschalidou et al. 2021a], which was originally introduced for scene synthesis but can be easily adapted to part-based object generation. In particular, instead of conditioning to a floor layout, we condition the generation on the object’s bounding box, as for our model. Finally, we also compare with IM-Net [Chen and Zhang 2019], which is an implicit-based generative model that does not reason about parts, hence not enabling part-level control.

Metrics To evaluate the quality of the generated shapes, we report the Coverage Score (COV) and the Minimum Matching Distance (MMD) [Achlioptas et al. 2018] using the Chamfer- L_2 distance (CD) between points sampled from real and generated shapes. To compute these metrics wrt. our part-based representation, we sample points on the surface of the union of the generated cuboids.

4.1 Shape Generation

We evaluate the performance of our model on the shape generation task on chairs, tables and lamps and perform category-specific training for our model and our baselines. Conditioned on different bounding boxes, our model can successfully synthesize meaningful part arrangements (see 4th column in Fig. 5, Fig. 6 and Fig. 11), which are fed to our blending network that combines them and yields plausible 3D meshes (see 5th column in Fig. 5, Fig. 6 and Fig. 11). We observe that PASTA consistently generates diverse and realistic part arrangements (Ours-Parts) for all object categories, which are, in turn, converted into meshes (Ours) that faithfully capture the initial part representation with cuboids. On the contrary, ATISS struggles to synthesize meaningful part sequences, i.e. the synthesized part arrangements consist of parts positioned in unnatural positions, especially for the case of chairs and tables. While synthesized objects sampled from PQ-NET and IM-NET are more realistic than the part arrangements produced by ATISS, they lack diversity, as indicated by the coverage score in Tab. 1. Note that our model, even without

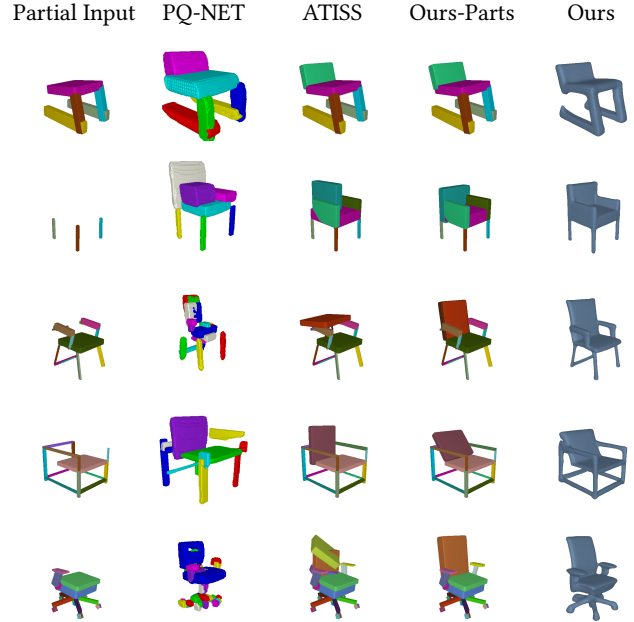


Fig. 7. **Shape Completion Results on Chairs.** Starting from partial chairs, we show completions of our model, ATISS and PQ-NET.

| Method | Representation | MMD-CD (\downarrow) | | | COV-CD ($\%$, \uparrow) | | |
|------------|----------------|-------------------------|-------------|-------------|------------------------------|--------------|--------------|
| | | Chair | Table | Lamp | Chair | Table | Lamp |
| PQ-Net | Implicit Parts | 4.69 | 3.64 | 4.55 | 35.77 | 42.31 | 53.33 |
| ATISS | Cuboids | 4.33 | 3.40 | 5.90 | 44.57 | 43.33 | 60.88 |
| Ours-Parts | Cuboids | 3.43 | 2.66 | 5.72 | 50.49 | 56.13 | 57.78 |
| Ours | Implicit | 3.11 | 2.33 | 5.58 | 49.00 | 58.56 | 51.00 |

Table 2. **Shape Completion.** We measure the MMD-CD (\downarrow) and the COV-CD (\uparrow) between the part-based representations of completed and real shapes from the test set.

the blending network (see Ours-Parts in Tab. 1), outperforms both PQ-NET and ATISS on chairs and tables on both metrics, while our complete architecture (see Ours in Tab. 1) outperforms also the non-part-based IM-NET on all object categories. For the case of lamps, we observe that our model outperforms all baselines wrt. MMD-CD, while performing on par with ATISS that achieves the highest score wrt. COV-CD. We hypothesize that ATISS performs better on the lamps category, as they typically consist of fewer components, hence making training and inference easier. Next, we evaluate the ability of our model and our baselines to generate plausible 3D shapes when jointly trained on multiple object categories, without any class conditioning. Again our model consistently produces plausible part arrangements that are more realistic and diverse than our baselines, as validated by our quantitative analysis in Tab. 1 (see 6th and 10th column). Fig. 12 provides a qualitative comparison of six objects generated with our model and our baselines.

4.2 Shape Completion

Starting from an incomplete sequence of parts, we evaluate whether our model and our baselines can complete the input sequence in a meaningful way. For this experiment, we only consider our part-based baselines and all models are trained in a category-specific

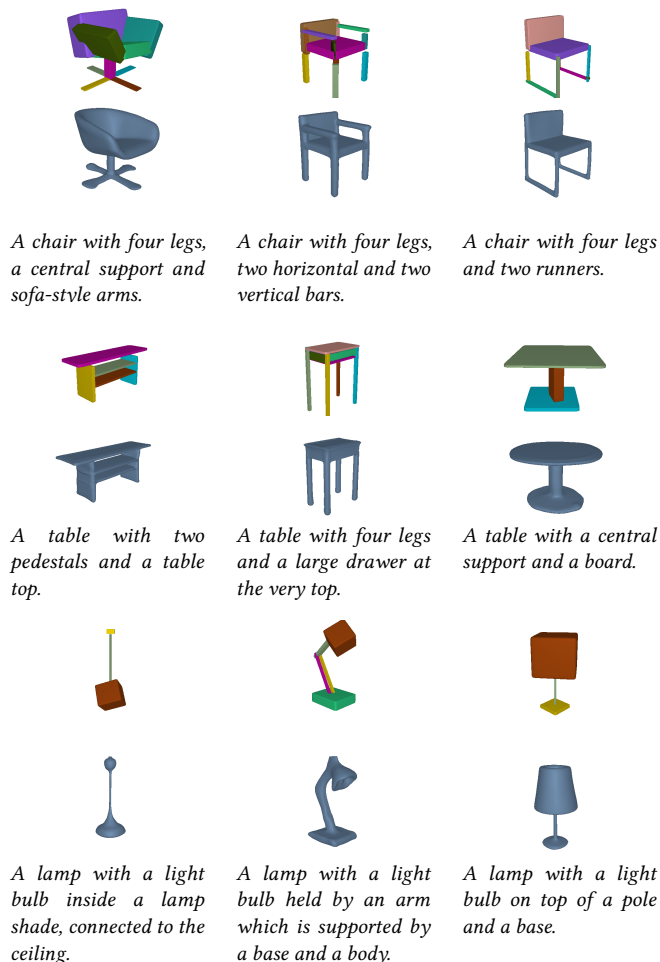


Fig. 8. **Text-guided Shape Generation.** Given different text descriptions our model can generate plausible 3D shapes of chairs, tables, and lamps.

manner. To ensure a fair comparison to PQ-NET, which is trained with 3D parts of arbitrary geometries, instead of conditioning their generation on the partial set of cuboids (illustrated in the 1st column of Fig. 7, Fig. 14 and Fig. 13), that is used for PASTA and ATISS, we utilize the corresponding 3D parts, that were used during PQ-NET’s training. From our qualitative evaluation, we observe that both ATISS and PQ-NET tend to generate non-realistic part arrangements, especially for the case of chairs (see unnatural back part for the 3rd and 6th chairs in the 3rd column of Fig. 7) and tables (see missing leg in the 2nd table in the 2nd column of Fig. 14). For the easier case of lamps (see Fig. 13), we observe that all methods can complete the partial object in a meaningful way. Note that, as PQ-NET relies on a sequence-to-sequence autoencoder to learn the part arrangements, there is no guarantee that the completed shape will contain the parts used for conditioning (see 3rd+4th row in Fig. 7, 2nd row in Fig. 14). Moreover, while for PASTA, the same model is used for both object completion as well as object generation, PQ-NET requires training a different model to perform the completion task.

To demonstrate that PASTA generates diverse part arrangements, we also visualize three generated completions of our model conditioned on the same partial input (see Fig. 9). We observe that our generations are consistently valid and diverse. The quantitative results for this experiment are summarized in Tab. 2. We note that our model outperforms all baselines both on chairs and tables wrt. both metrics. For the case of lamps, ATISS outperforms all methods wrt. COV-CD, while being worse than all in terms of MMD-CD.

4.3 Applications

In this section, we present several applications of our model, such as conditional generation from text and images. In both experiments, our model is trained in a category-specific manner.

Language-guided Generation For this experiment, we use the part labels provided in PartNet [Mo et al. 2019b] and generate utterances that describe the part-based structure of each object. We train a variant of our model that conditions on CLIP [Radford et al. 2021] embeddings produced from our textual descriptions in addition to the object bounding box as described in Sec. 3.5. In Fig. 8, we provide text-guided generations of our model and observe note that they consistently match the input text (e.g. the table with the two pedestals, or the lamp connected to the ceiling).

Image-guided Generation: We now test the ability of our model to perform image-guided generation using the same model that was trained for language-guided generation, without any re-training. In particular, we take advantage of the CLIP’s joint latent space, and condition our model on image embeddings produced by CLIP’s image encoder. Fig. 10 shows examples of image-guided synthesis. While PASTA was never trained with images, we showcase that it generates shapes of various object categories that faithfully match the input image. Notably, the recovered parts capture fine geometric details such as the three legs of the first table in the Fig. 10.

5 CONCLUSION

In this paper, we introduced PASTA a part-aware generative model for 3D shapes. Our architecture consists of two main components: the *object generator* that autoregressively generates objects as sequences of labelled cuboids and the *blending network* that combines a sequence of cuboidal primitives and synthesizes a high-quality implicit shape. Unlike traditional autoregressive models that are trained with teacher forcing, we demonstrate that relying on scheduled sampling [Bengio et al. 2015] improves the generation performance of our model. Our experiments, showcase that PASTA generates more meaningful part arrangements and plausible 3D objects than both part-based [Paschalidou et al. 2021a; Wu et al. 2020] and non part-based generative models [Chen and Zhang 2019]. In future work, we plan to extend our architecture to generate parts with textures. Note that this is a straight-forward extension of our method if we simply replace our blending network with a NeRF-based decoder [Mildenhall et al. 2020] that instead of predicting occupancies, predicts colors and opacities. Another exciting direction for future research, is to explore learning such part-based autoregressive models without explicit part annotations.

REFERENCES

- Martín Abadi. 2016. TensorFlow: learning functions at scale. In *Proceedings of the 21st ACM SIGPLAN International Conference on Functional Programming*.
- Panos Achlioptas, Olga Diamanti, Ioannis Mitliagkas, and Leonidas J. Guibas. 2018. Learning Representations and Generative Models for 3D Point Clouds. In *Proc. of the International Conf. on Machine Learning (ICML)*.
- Yazeed Alharbi and Peter Wonka. 2020. Disentangled Image Generation Through Structured Noise Injection. In *Proc. IEEE Conf. on Computer Vision and Pattern Recognition (CVPR)*. 5133–5141.
- Matan Atzmon and Yaron Lipman. 2020. SAL: Sign Agnostic Learning of Shapes From Raw Data. In *Proc. IEEE Conf. on Computer Vision and Pattern Recognition (CVPR)*. 2562–2571.
- Jason Bailey. 2020. The tools of generative art, from Flash to neural networks. *Art in America* 8 (2020).
- Samy Bengio, Oriol Vinyals, Navdeep Jaitly, and Noam Shazeer. 2015. Scheduled Sampling for Sequence Prediction with Recurrent Neural Networks. In *Advances in Neural Information Processing Systems (NIPS)*.
- Andrew Brock, Jeff Donahue, and Karen Simonyan. 2019. Large Scale GAN Training for High Fidelity Natural Image Synthesis. In *Proc. of the International Conf. on Learning Representations (ICLR)*.
- André Brock, Theodore Lim, James M. Ritchie, and Nick Weston. 2016. Generative and Discriminative Voxel Modeling with Convolutional Neural Networks. *arXiv.org* 1608.04236 (2016).
- Ruojin Cai, Guandao Yang, Hadar Averbuch-Elor, Zekun Hao, Serge J. Belongie, Noah Snavely, and Bharath Hariharan. 2020. Learning Gradient Fields for Shape Generation. In *Proc. of the European Conf. on Computer Vision (ECCV)*.
- Eric R. Chan, Connor Z. Lin, Matthew A. Chan, Koki Nagano, Boxiao Pan, Shalini De Mello, Orazio Gallo, Leonidas J. Guibas, Jonathan Tremblay, Sameh Khamis, Tero Karras, and Gordon Wetzstein. 2022. Efficient Geometry-aware 3D Generative Adversarial Networks. In *Proc. IEEE Conf. on Computer Vision and Pattern Recognition (CVPR)*.
- Eric R. Chan, Marco Monteiro, Petr Kellnhofer, Jiajun Wu, and Gordon Wetzstein. 2021. Pi-GAN: Periodic Implicit Generative Adversarial Networks for 3D-Aware Image Synthesis. In *Proc. IEEE Conf. on Computer Vision and Pattern Recognition (CVPR)*.
- Angel X. Chang, Thomas A. Funkhouser, Leonidas J. Guibas, Pat Hanrahan, Qi-Xing Huang, Zimo Li, Silvio Savarese, Manolis Savva, Shuran Song, Hao Su, Jianxiong Xiao, Li Yi, and Fisher Yu. 2015. ShapeNet: An Information-Rich 3D Model Repository. *arXiv.org* 1512.03012 (2015).
- Mark Chen, Alec Radford, Rewon Child, Jeffrey Wu, Heewoo Jun, David Luan, and Ilya Sutskever. 2020a. Generative Pretraining From Pixels. In *Proc. of the International Conf. on Machine Learning (ICML)*.
- Zhiqin Chen, Andrea Tagliasacchi, and Hao Zhang. 2020b. BSP-Net: Generating Compact Meshes via Binary Space Partitioning. In *Proc. IEEE Conf. on Computer Vision and Pattern Recognition (CVPR)*. 42–51.
- Zhiqin Chen and Hao Zhang. 2019. Learning Implicit Fields for Generative Shape Modeling. In *Proc. IEEE Conf. on Computer Vision and Pattern Recognition (CVPR)*.
- Yunjeong Choi, Min-Je Choi, Munyoung Kim, Jung-Woo Ha, Sunghun Kim, and Jaegul Choo. 2018. StarGAN: Unified Generative Adversarial Networks for Multi-Domain Image-to-Image Translation. In *Proc. IEEE Conf. on Computer Vision and Pattern Recognition (CVPR)*.
- Christopher Bongsoo Choy, Danfei Xu, JunYoung Gwak, Kevin Chen, and Silvio Savarese. 2016. 3D-R2N2: A Unified Approach for Single and Multi-view 3D Object Reconstruction. In *Proc. of the European Conf. on Computer Vision (ECCV)*.
- Boyang Deng, Kyle Genova, Soroosh Yazdani, Sofien Bouaziz, Geoffrey Hinton, and Andrea Tagliasacchi. 2020. CvxNets: Learnable Convex Decomposition. *Proc. IEEE Conf. on Computer Vision and Pattern Recognition (CVPR)* (2020).
- Theo Deprelle, Thibault Groueix, Matthew Fisher, Vladimir G Kim, Bryan C Russell, and Mathieu Aubry. 2019. Learning elementary structures for 3D shape generation and matching. In *Advances in Neural Information Processing Systems (NIPS)*.
- Prafulla Dhariwal, Heewoo Jun, Christine Payne, Jong Wook Kim, Alec Radford, and Ilya Sutskever. 2020. Jukebox: A Generative Model for Music. *arXiv.org* (2020).
- Laurent Dinh, David Krueger, and Yoshua Bengio. 2015. NICE: Non-linear Independent Components Estimation. In *Proc. of the International Conf. on Learning Representations (ICLR)*.
- Anastasia Dubrovina, Fei Xia, Panos Achlioptas, Mira Shalah, Raphaël Groskot, and Leonidas J. Guibas. 2019. Composite Shape Modeling via Latent Space Factorization. In *Proc. of the IEEE International Conf. on Computer Vision (ICCV)*. IEEE, 8139–8148.
- Kevin Ellis, Daniel Ritchie, Armando Solar-Lezama, and Joshua B. Tenenbaum. 2018. Learning to Infer Graphics Programs from Hand-Drawn Images. In *Advances in Neural Information Processing Systems (NIPS)*.
- Patrick Esser, Robin Rombach, and Björn Ommer. 2021. Taming Transformers for High-Resolution Image Synthesis. *Proc. IEEE Conf. on Computer Vision and Pattern Recognition (CVPR)*.
- Haoqiang Fan, Hao Su, and Leonidas J. Guibas. 2017. A Point Set Generation Network for 3D Object Reconstruction from a Single Image. *Proc. IEEE Conf. on Computer Vision and Pattern Recognition (CVPR)* (2017).
- Matheus Gadelha, Giorgio Gori, Duygu Ceylan, Radomir Mech, Nathan Carr, Tamy Boubekeur, Rui Wang, and Subhransu Maji. 2020. Learning Generative Models of Shape Handles. In *Proc. IEEE Conf. on Computer Vision and Pattern Recognition (CVPR)*.
- Matheus Gadelha, Subhransu Maji, and Rui Wang. 2017. 3D Shape Induction from 2D Views of Multiple Objects. In *Proc. of the International Conf. on 3D Vision (3DV)*.
- Jun Gao, Tianchang Shen, Zian Wang, Wenzheng Chen, Kangxue Yin, Daiqing Li, Or Litany, Zan Gojic, and Sanja Fidler. 2022. GET3D: A Generative Model of High Quality 3D Textured Shapes Learned from Images. In *Advances in Neural Information Processing Systems (NeurIPS)*.
- Kyle Genova, Forrester Cole, Avneesh Sud, Aaron Sarna, and Thomas A. Funkhouser. 2020. Local Deep Implicit Functions for 3D Shape. In *Proc. IEEE Conf. on Computer Vision and Pattern Recognition (CVPR)*.
- Kyle Genova, Forrester Cole, Daniel Vlasic, Aaron Sarna, William T Freeman, and Thomas Funkhouser. 2019. Learning Shape Templates with Structured Implicit Functions. In *Proc. of the IEEE International Conf. on Computer Vision (ICCV)*.
- Ian J. Goodfellow, Jean Pouget-Abadie, Mehdi Mirza, Bing Xu, David Warde-Farley, Sherjil Ozair, Aaron C. Courville, and Yoshua Bengio. 2014. Generative Adversarial Nets. In *Advances in Neural Information Processing Systems (NIPS)*.
- Amos Gropp, Lior Yariv, Niv Haim, Matan Atzmon, and Yaron Lipman. 2020. Implicit Geometric Regularization for Learning Shapes. In *Proc. of the International Conf. on Machine Learning (ICML)*.
- Thibault Groueix, Matthew Fisher, Vladimir G. Kim, Bryan C. Russell, and Mathieu Aubry. 2018. AtlasNet: A Papier-Mâché Approach to Learning 3D Surface Generation. In *Proc. IEEE Conf. on Computer Vision and Pattern Recognition (CVPR)*.
- Jiatao Gu, Lingjie Liu, Peng Wang, and Christian Theobalt. 2022. StyleNeRF: A Style-based 3D Aware Generator for High-resolution Image Synthesis. In *Proc. of the International Conf. on Learning Representations (ICLR)*.
- Zekun Hao, Hadar Averbuch-Elor, Noah Snavely, and Serge J. Belongie. 2020. DualSDF: Semantic Shape Manipulation Using a Two-Level Representation. In *Proc. IEEE Conf. on Computer Vision and Pattern Recognition (CVPR)*.
- Phillip Henzler, Niloy J Mitra, , and Tobias Ritschel. 2019. Escaping Plato’s Cave: 3D Shape From Adversarial Rendering. In *Proc. of the IEEE International Conf. on Computer Vision (ICCV)*.
- Amir Hertz, Or Perel, Raja Giryes, Olga Sorkine-Hornung, and Daniel Cohen-Or. 2022. SPAGHETTI: editing implicit shapes through part aware generation. *ACM Trans. on Graphics* (2022).
- Martin Heusel, Hubert Ramsauer, Thomas Unterthiner, Bernhard Nessler, and Sepp Hochreiter. 2017. GANs Trained by a Two Time-scale Update Rule Converge to a Local Nash Equilibrium. In *Advances in Neural Information Processing Systems (NIPS)*.
- Sepp Hochreiter and Jürgen Schmidhuber. 1997. Long Short-Term Memory. *Neural Computation* 9, 8 (1997), 1735–1780.
- Xinyu Huang, Peng Wang, Xinjing Cheng, Dingfu Zhou, Qichuan Geng, and Ruigang Yang. 2018. The ApolloScape Open Dataset for Autonomous Driving and its Application. *arXiv.org* 1803.06184 (2018).
- Moritz Ibing, Gregor Kobsik, and Leif Kobbelt. 2021. Octree Transformer: Autoregressive 3D Shape Generation on Hierarchically Structured Sequences. *arXiv.org* (2021).
- Phillip Isola, Jun-Yan Zhu, Tinghui Zhou, and Alexei A. Efros. 2017. Image-to-Image Translation with Conditional Adversarial Networks. In *Proc. IEEE Conf. on Computer Vision and Pattern Recognition (CVPR)*.
- Li Jiang, Shaoshuai Shi, Xiaojuan Qi, and Jiaya Jia. 2018. GAL: Geometric Adversarial Loss for Single-View 3D-Object Reconstruction. In *Proc. of the European Conf. on Computer Vision (ECCV)*.
- Angjoo Kanazawa, Shubham Tulsiani, Alexei A. Efros, and Jitendra Malik. 2018. Learning Category-Specific Mesh Reconstruction from Image Collections. In *Proc. of the European Conf. on Computer Vision (ECCV)*.
- Tero Karras, Samuli Laine, and Timo Aila. 2019. A Style-Based Generator Architecture for Generative Adversarial Networks. In *Proc. IEEE Conf. on Computer Vision and Pattern Recognition (CVPR)*.
- Tero Karras, Samuli Laine, Miika Aittala, Janne Hellsten, Jaakko Lehtinen, and Timo Aila. 2020. Analyzing and Improving the Image Quality of StyleGAN. (2020).
- Angelos Katharopoulos, Apoorv Vyas, Nikolaos Pappas, and François Fleuret. 2020. Transformers are RNNs: Fast Autoregressive Transformers with Linear Attention. In *Proc. of the International Conf. on Machine Learning (ICML)*.
- Diederik P. Kingma and Jimmy Ba. 2015. Adam: A Method for Stochastic Optimization. In *Proc. of the International Conf. on Learning Representations (ICLR)*.
- Diederik P. Kingma and Max Welling. 2014. Auto-Encoding Variational Bayes. *Proc. of the International Conf. on Learning Representations (ICLR)* (2014).
- Jun Li, Kai Xu, Siddhartha Chaudhuri, Ersin Yumer, Hao (Richard) Zhang, and Leonidas J. Guibas. 2017. GRASS: generative recursive autoencoders for shape structures. *ACM Trans. on Graphics* 36, 4 (2017).
- Ruihui Li, Xianzhi Li, Ka-Hei Hui, and Chi-Wing Fu. 2021. SP-GAN: sphere-guided 3D shape generation and manipulation. *ACM Trans. on Graphics* (2021).
- Yiyi Liao, Simon Donne, and Andreas Geiger. 2018. Deep Marching Cubes: Learning Explicit Surface Representations. In *Proc. IEEE Conf. on Computer Vision and Pattern Recognition (CVPR)* (2018).

- Recognition (CVPR).
- Yiyi Liao, Katja Schwarz, Lars M. Mescheder, and Andreas Geiger. 2020. Towards Unsupervised Learning of Generative Models for 3D Controllable Image Synthesis. *Proc. IEEE Conf. on Computer Vision and Pattern Recognition (CVPR)* (2020).
- Huan Ling, Karsten Kreis, Daqing Li, Seung Wook Kim, Antonio Torralba, and Sanja Fidler. 2021. EditGAN: High-Precision Semantic Image Editing. In *Advances in Neural Information Processing Systems (NIPS)*.
- Minghua Liu, Minhyuk Sung, Radomir Mech, and Hao Su. 2021. DeepMetaHandles: Learning Deformation Meta-Handles of 3D Meshes With Biharmonic Coordinates. In *Proc. IEEE Conf. on Computer Vision and Pattern Recognition (CVPR)*.
- Yunchao Liu, Zheng Wu, Daniel Ritchie, William T Freeman, Joshua B Tenenbaum, and Jiajun Wu. 2019. Learning to Describe Scenes with Programs. In *Proc. of the International Conf. on Learning Representations (ICLR)*.
- William E. Lorensen and Harvey E. Cline. 1987. Marching Cubes: A High Resolution 3D Surface Construction Algorithm. In *ACM Trans. on Graphics*.
- Andrew Luo, Tianqin Li, Wen-Hao Zhang, and Tai Sing Lee. 2021. SurfGen: Adversarial 3D Shape Synthesis with Explicit Surface Discriminators. In *Proc. of the IEEE International Conf. on Computer Vision (ICCV)*.
- Shitong Luo and Wei Hu. 2021. Diffusion Probabilistic Models for 3D Point Cloud Generation. In *Proc. IEEE Conf. on Computer Vision and Pattern Recognition (CVPR)*.
- Lars Mescheder, Michael Oechsle, Michael Niemeyer, Sebastian Nowozin, and Andreas Geiger. 2019. Occupancy Networks: Learning 3D Reconstruction in Function Space. In *Proc. IEEE Conf. on Computer Vision and Pattern Recognition (CVPR)*.
- Mateusz Michalkiewicz, Jhony K Pontes, Dominic Jack, Mahsa Baktashmotlagh, and Anders Eriksson. 2019. Implicit Surface Representations as Layers in Neural Networks. In *Proc. of the IEEE International Conf. on Computer Vision (ICCV)*.
- Tsvetomila Mihaylova and André F. T. Martins. 2019. Scheduled Sampling for Transformers. *arXiv.org* (2019).
- Ben Mildenhall, Pratul P Srinivasan, Matthew Tancik, Jonathan T Barron, Ravi Ramamoorthi, and Ren Ng. 2020. NeRF: Representing scenes as neural radiance fields for view synthesis. In *Proc. of the European Conf. on Computer Vision (ECCV)*.
- Paritosh Mittal, Yen-Chi Cheng, Maneesh Singh, and Shubham Tulsiani. 2022. AutoSDF: Shape Priors for 3D Completion, Reconstruction and Generation. In *Proc. IEEE Conf. on Computer Vision and Pattern Recognition (CVPR)*.
- Kaichun Mo, Paul Guerrero, Li Yi, Hao Su, Peter Wonka, Niloy Mitra, and Leonidas J. Guibas. 2019a. StructureNet: Hierarchical Graph Networks for 3D Shape Generation. In *ACM Trans. on Graphics*.
- Kaichun Mo, Paul Guerrero, Li Yi, Hao Su, Peter Wonka, Niloy J. Mitra, and Leonidas J. Guibas. 2020. StructEdit: Learning Structural Shape Variations. In *Proc. IEEE Conf. on Computer Vision and Pattern Recognition (CVPR)*.
- Kaichun Mo, Shilin Zhu, Angel X Chang, Li Yi, Subarna Tripathi, Leonidas J Guibas, and Hao Su. 2019b. PartNet: A Large-scale Benchmark for Fine-grained and Hierarchical Part-level 3D Object Understanding. In *Proc. IEEE Conf. on Computer Vision and Pattern Recognition (CVPR)*.
- Charlie Nash, Yaroslav Ganin, S. M. Ali Eslami, and Peter W. Battaglia. 2020. PolyGen: An Autoregressive Generative Model of 3D Meshes. In *Proc. of the International Conf. on Machine Learning (ICML)*.
- Thu Nguyen-Phuoc, Chuan Li, Lucas Theis, Christian Richardt, and Yong-Liang Yang. 2019. HoloGAN: Unsupervised Learning of 3D Representations From Natural Images. In *Proc. of the IEEE International Conf. on Computer Vision (ICCV)*.
- Thu Nguyen-Phuoc, Christian Richardt, Long Mai, Yong-Liang Yang, and Niloy J. Mitra. 2020. BlockGAN: Learning 3D Object-aware Scene Representations from Unlabelled Images. In *Advances in Neural Information Processing Systems (NeurIPS)*.
- Michael Niemeyer, Lars Mescheder, Michael Oechsle, and Andreas Geiger. 2020. Differentiable Volumetric Rendering: Learning Implicit 3D Representations without 3D Supervision. In *Proc. IEEE Conf. on Computer Vision and Pattern Recognition (CVPR)*.
- Chengjie Niu, Jun Li, and Kai Xu. 2018. Im2Struct: Recovering 3D Shape Structure from a Single RGB Image. In *Proc. IEEE Conf. on Computer Vision and Pattern Recognition (CVPR)*.
- Myle Ott, Sergey Edunov, David Grangier, and Michael Auli. 2018. Scaling Neural Machine Translation. In *Proceedings of the Third Conference on Machine Translation: Research Papers, WMT 2018, Belgium, Brussels, October 31 - November 1, 2018*.
- Junyi Pan, Xiaoguang Han, Weikai Chen, Jiapeng Tang, and Kui Jia. 2019. Deep Mesh Reconstruction From Single RGB Images via Topology Modification Networks. In *Proc. of the IEEE International Conf. on Computer Vision (ICCV)*.
- Jeong Joon Park, Peter Florence, Julian Straub, Richard A. Newcombe, and Steven Lovegrove. 2019. DeepSDF: Learning Continuous Signed Distance Functions for Shape Representation. In *Proc. IEEE Conf. on Computer Vision and Pattern Recognition (CVPR)*.
- Niki Parmar, Ashish Vaswani, Jakob Uszkoreit, Lukasz Kaiser, Noam Shazeer, Alexander Ku, and Dustin Tran. 2018. Image Transformer. In *Proc. of the International Conf. on Machine Learning (ICML)*.
- Despoina Paschalidou, Amlan Kar, Maria Shugrina, Karsten Kreis, Andreas Geiger, and Sanja Fidler. 2021a. ATISS: Autoregressive Transformers for Indoor Scene Synthesis. In *Advances in Neural Information Processing Systems (NeurIPS)*.
- Despoina Paschalidou, Angelos Katharopoulos, Andreas Geiger, and Sanja Fidler. 2021b. Neural Parts: Learning Expressive 3D Shape Abstractions with Invertible Neural Networks. In *Proc. IEEE Conf. on Computer Vision and Pattern Recognition (CVPR)*.
- Despoina Paschalidou, Ali Osman Ulusoy, and Andreas Geiger. 2019. Superquadrics Revisited: Learning 3D Shape Parsing beyond Cuboids. In *Proc. IEEE Conf. on Computer Vision and Pattern Recognition (CVPR)*.
- Despoina Paschalidou, Luc van Gool, and Andreas Geiger. 2020. Learning Unsupervised Hierarchical Part Decomposition of 3D Objects from a Single RGB Image. In *Proc. IEEE Conf. on Computer Vision and Pattern Recognition (CVPR)*.
- Adam Paszke, Abhishek Chaurasia, Sangpil Kim, and Eugenio Durruti. 2016. ENet: A Deep Neural Network Architecture for Real-Time Semantic Segmentation. *arXiv.org* 1606.02147 (2016).
- Dario Pavlo, Jonas Kohler, Thomas Hofmann, and Aurélien Lucchi. 2021. Learning Generative Models of Textured 3D Meshes from Real-World Images. In *Proc. of the IEEE International Conf. on Computer Vision (ICCV)*.
- Dario Pavlo, Graham Spinks, Thomas Hofmann, Marie-Francine Moens, and Aurélien Lucchi. 2020. Convolutional Generation of Textured 3D Meshes. In *Advances in Neural Information Processing Systems (NeurIPS)*.
- Charles R Qi, Li Yi, Hao Su, and Leonidas J Guibas. 2017. PointNet++: Deep Hierarchical Feature Learning on Point Sets in a Metric Space. In *Advances in Neural Information Processing Systems (NIPS)*.
- Alec Radford, Jong Wook Kim, Chris Hallacy, Aditya Ramesh, Gabriel Goh, Sandhini Agarwal, Girish Sastry, Amanda Askell, Pamela Mishkin, Jack Clark, et al. 2021. Learning transferable visual models from natural language supervision. In *International Conference on Machine Learning*.
- Danilo Jimenez Rezende, S. M. Ali Eslami, Shakir Mohamed, Peter Battaglia, Max Jaderberg, and Nicolas Heess. 2016. Unsupervised Learning of 3D Structure from Images. In *Advances in Neural Information Processing Systems (NIPS)*.
- Gernot Riegler, Ali Osman Ulusoy, and Andreas Geiger. 2017. OctNet: Learning Deep 3D Representations at High Resolutions. In *Proc. IEEE Conf. on Computer Vision and Pattern Recognition (CVPR)*.
- Daniel Ritchie, Kai Wang, and Yu-An Lin. 2019. Fast and Flexible Indoor Scene Synthesis via Deep Convolutional Generative Models. In *Proc. IEEE Conf. on Computer Vision and Pattern Recognition (CVPR)*.
- Shunsuke Saito, Zeng Huang, Ryota Natsume, Shigeo Morishima, Angjoo Kanazawa, and Hao Li. 2019. PIFu: Pixel-Aligned Implicit Function for High-Resolution Clothed Human Digitization. In *Proc. of the IEEE International Conf. on Computer Vision (ICCV)*.
- Tim Salimans, Andrej Karpathy, Xi Chen, and Diederik P. Kingma. 2017. PixelCNN++: Improving the PixelCNN with Discretized Logistic Mixture Likelihood and Other Modifications. In *Proc. of the International Conf. on Learning Representations (ICLR)*.
- Mike Schuster and Kuldeep K. Paliwal. 1997. Bidirectional recurrent neural networks. *IEEE Trans. Signal Process.* (1997).
- Katja Schwarz, Yiyi Liao, Michael Niemeyer, and Andreas Geiger. 2020. GRAF: Generative Radiance Fields for 3D-Aware Image Synthesis. In *Advances in Neural Information Processing Systems (NeurIPS)*.
- Gopal Sharma, Rishabh Goyal, Difan Liu, Evangelos Kalogerakis, and Subhransu Maji. 2018. CSGNet: Neural Shape Parser for Constructive Solid Geometry. In *Proc. IEEE Conf. on Computer Vision and Pattern Recognition (CVPR)*.
- Peter Shaw, Jakob Uszkoreit, and Ashish Vaswani. 2018. Self-Attention with Relative Position Representations. In *Proceedings of the 2018 Conference of the North American Chapter of the Association for Computational Linguistics: Human Language Technologies, NAACL-HLT, New Orleans, Louisiana, USA, June 1-6, 2018, Volume 2 (Short Papers)*.
- Yujun Shen, Jinjin Gu, Xiaoou Tang, and Bolei Zhou. 2020. Interpreting the Latent Space of GANs for Semantic Face Editing. In *Proc. IEEE Conf. on Computer Vision and Pattern Recognition (CVPR)*.
- David Stutz and Andreas Geiger. 2018. Learning 3D Shape Completion from Laser Scan Data with Weak Supervision. In *Proc. IEEE Conf. on Computer Vision and Pattern Recognition (CVPR)*.
- Towaki Takikawa, Joey Litalien, Kangxue Yin, Karsten Kreis, Charles T. Loop, Derek Nowrouzezahrai, Alec Jacobson, Morgan McGuire, and Sanja Fidler. 2021. Neural Geometric Level of Detail: Real-Time Rendering With Implicit 3D Shapes. In *Proc. IEEE Conf. on Computer Vision and Pattern Recognition (CVPR)*.
- Hugues Thomas, Charles R. Qi, Jean-Emmanuel Deschard, Beatriz Marcotegui, François Goulette, and Leonidas J. Guibas. 2019. KPConv: Flexible and Deformable Convolution for Point Clouds. In *Proc. of the IEEE International Conf. on Computer Vision (ICCV)*.
- Yonglong Tian, Andrew Luo, Xingyuan Sun, Kevin Ellis, William T Freeman, Joshua B Tenenbaum, and Jiajun Wu. 2019. Learning to Infer and Execute 3D Shape Programs. In *Proc. of the International Conf. on Learning Representations (ICLR)*.
- Shubham Tulsiani and Abhinav Gupta. 2021. PixelTransformer: Sample Conditioned Signal Generation. In *Proc. of the International Conf. on Machine Learning (ICML)*.
- Shubham Tulsiani, Hao Su, Leonidas J. Guibas, Alexei A. Efros, and Jitendra Malik. 2017. Learning Shape Abstractions by Assembling Volumetric Primitives. In *Proc. IEEE Conf. on Computer Vision and Pattern Recognition (CVPR)*.

- Aaron van den Oord, Sander Dieleman, Heiga Zen, Karen Simonyan, Oriol Vinyals, Alex Graves, Nal Kalchbrenner, Andrew W. Senior, and Koray Kavukcuoglu. 2016. WaveNet: A Generative Model for Raw Audio. In *The 9th ISCA Speech Synthesis Workshop, Sunnyvale, CA, USA, 13-15 September 2016*.
- Ashish Vaswani, Noam Shazeer, Niki Parmar, Jakob Uszkoreit, Llion Jones, Aidan N. Gomez, Lukasz Kaiser, and Illia Polosukhin. 2017. Attention is All you Need. In *Advances in Neural Information Processing Systems (NIPS)*, 5998–6008.
- Binxu Wang and Carlos R. Ponce. 2021. A Geometric Analysis of Deep Generative Image Models and Its Applications. In *Proc. of the International Conf. on Learning Representations (ICLR)*.
- Nanyang Wang, Yinda Zhang, Zhuwen Li, Yanwei Fu, Wei Liu, and Yu-Gang Jiang. 2018b. Pixel2mesh: Generating 3d mesh models from single rgb images. In *Proc. of the European Conf. on Computer Vision (ECCV)*.
- Ting-Chun Wang, Ming-Yu Liu, Jun-Yan Zhu, Andrew Tao, Jan Kautz, and Bryan Catanzaro. 2018a. High-Resolution Image Synthesis and Semantic Manipulation With Conditional GANs. In *Proc. IEEE Conf. on Computer Vision and Pattern Recognition (CVPR)*.
- Xinpeng Wang, Chandan Yeshwanth, and Matthias Nießner. 2020. SceneFormer: Indoor Scene Generation with Transformers. *arXiv.org* (2020).
- Yanzhen Wang, Kai Xu, Jun Li, Hao Zhang, Ariel Shamir, Ligang Liu, Zhi-Quan Cheng, and Yueshan Xiong. 2011. Symmetry Hierarchy of Man-Made Objects. In *EURO-GRAPHICS*.
- Rundi Wu, Yixin Zhuang, Kai Xu, Hao Zhang, and Baoquan Chen. 2020. PQ-NET: A Generative Part Seq2Seq Network for 3D Shapes. In *Proc. IEEE Conf. on Computer Vision and Pattern Recognition (CVPR)*.
- Haozhe Xie, Hongxun Yao, Xiaoshuai Sun, Shangchen Zhou, and Shengping Zhang. 2019. Pix2Vox: Context-Aware 3D Reconstruction From Single and Multi-View Images. In *Proc. of the IEEE International Conf. on Computer Vision (ICCV)*.
- Qiangeng Xu, Weiyue Wang, Duygu Ceylan, Radomir Mech, and Ulrich Neumann. 2019. DISN: Deep Implicit Surface Network for High-quality Single-view 3D Reconstruction. In *Advances in Neural Information Processing Systems (NIPS)*.
- Guandao Yang, Xun Huang, Zekun Hao, Ming-Yu Liu, Serge J. Belongie, and Bharath Hariharan. 2019. PointFlow: 3D Point Cloud Generation with Continuous Normalizing Flows. In *Proc. of the IEEE International Conf. on Computer Vision (ICCV)*.
- Chun-Han Yao, Wei-Chih Hung, Varun Jampani, and Ming-Hsuan Yang. 2021. Discovering 3D Parts from Image Collections. In *Proc. of the IEEE International Conf. on Computer Vision (ICCV)*.
- Chun-Han Yao, Wei-Chih Hung, Yuanzhen Li, Michael Rubinstein, Ming-Hsuan Yang, and Varun Jampani. 2022. LASSIE: Learning Articulated Shapes from Sparse Image Ensemble via 3D Part Discovery. *arXiv.org abs/2207.03434* (2022).
- Lior Yariv, Yoni Kasten, Dror Moran, Meirav Galun, Matan Atzmon, Ronen Basri, and Yaron Lipman. 2020. Multiview Neural Surface Reconstruction by Disentangling Geometry and Appearance. In *Advances in Neural Information Processing Systems (NIPS)*.
- Xumin Yu, Yongming Rao, Ziyi Wang, Zuyan Liu, Jiwen Lu, and Jie Zhou. 2021. PoinTr: Diverse Point Cloud Completion with Geometry-Aware Transformers. In *Proc. of the IEEE International Conf. on Computer Vision (ICCV)*.
- Yuxuan Zhang, Wenzheng Chen, Huan Ling, Jun Gao, Yinan Zhang, Antonio Torralba, and Sanja Fidler. 2021. Image GANs meet Differentiable Rendering for Inverse Graphics and Interpretable 3D Neural Rendering. In *Proc. of the International Conf. on Learning Representations (ICLR)*.
- Linqi Zhou, Yilun Du, and Jiajun Wu. 2021. 3D Shape Generation and Completion through Point-Voxel Diffusion. In *Proc. of the IEEE International Conf. on Computer Vision (ICCV)*.
- Yi Zhou, Connelly Barnes, Jingwan Lu, Jimei Yang, and Hao Li. 2019. On the Continuity of Rotation Representations in Neural Networks. In *Proc. IEEE Conf. on Computer Vision and Pattern Recognition (CVPR)*.
- Xizhou Zhu, Yujie Wang, Jifeng Dai, Lu Yuan, and Yichen Wei. 2017. Flow-Guided Feature Aggregation for Video Object Detection. In *Proc. of the IEEE International Conf. on Computer Vision (ICCV)*.
- Chuhang Zou, Ersin Yumer, Jimei Yang, Duygu Ceylan, and Derek Hoiem. 2017. 3D-PRNN: Generating Shape Primitives with Recurrent Neural Networks. In *Proc. of the IEEE International Conf. on Computer Vision (ICCV)*.

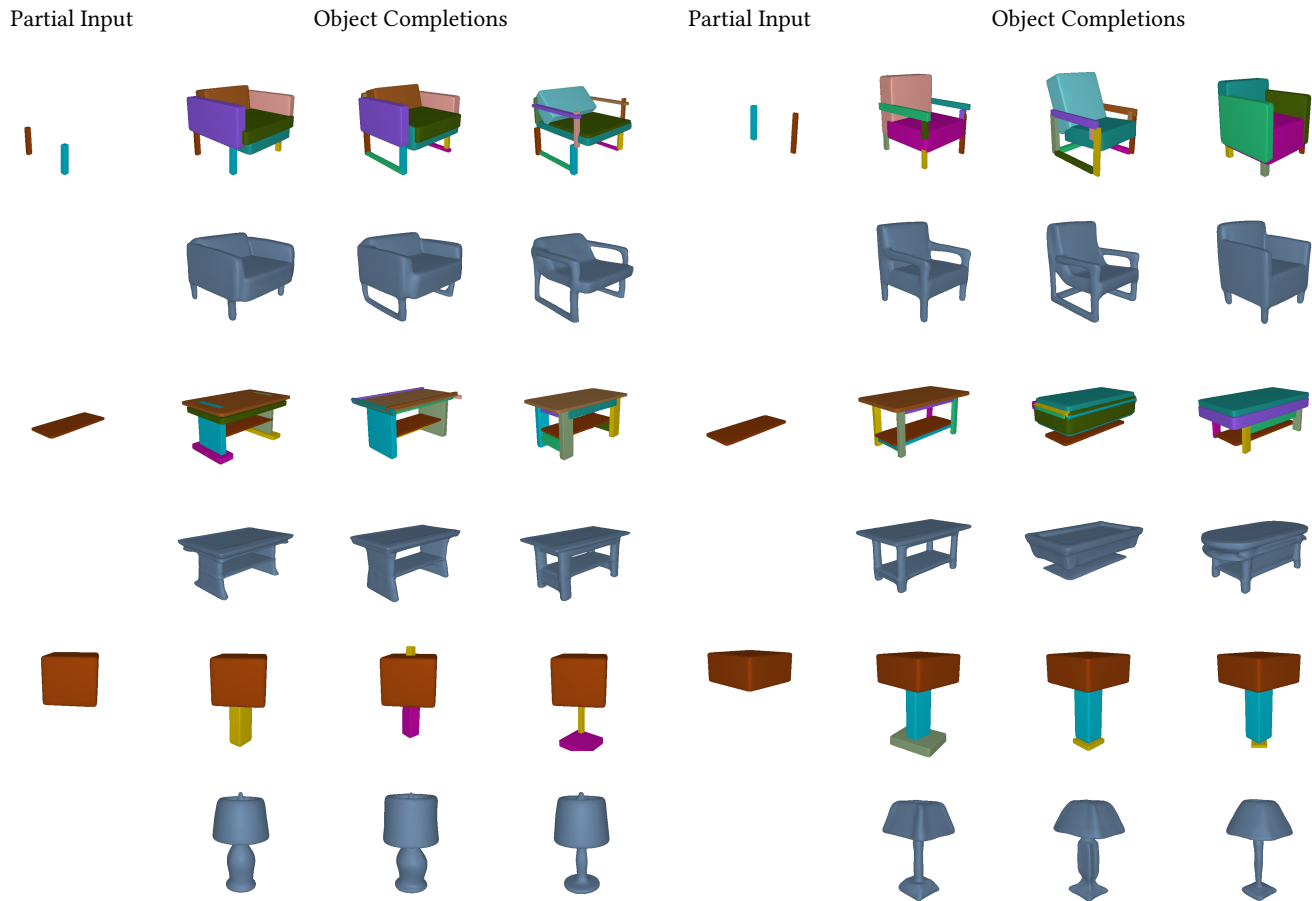


Fig. 9. **Diversity of Object Completions.** Starting from a partial object, we show several completions using our model. The first two rows show completion results for chairs, the third and fourth for tables and the last two for lamps.

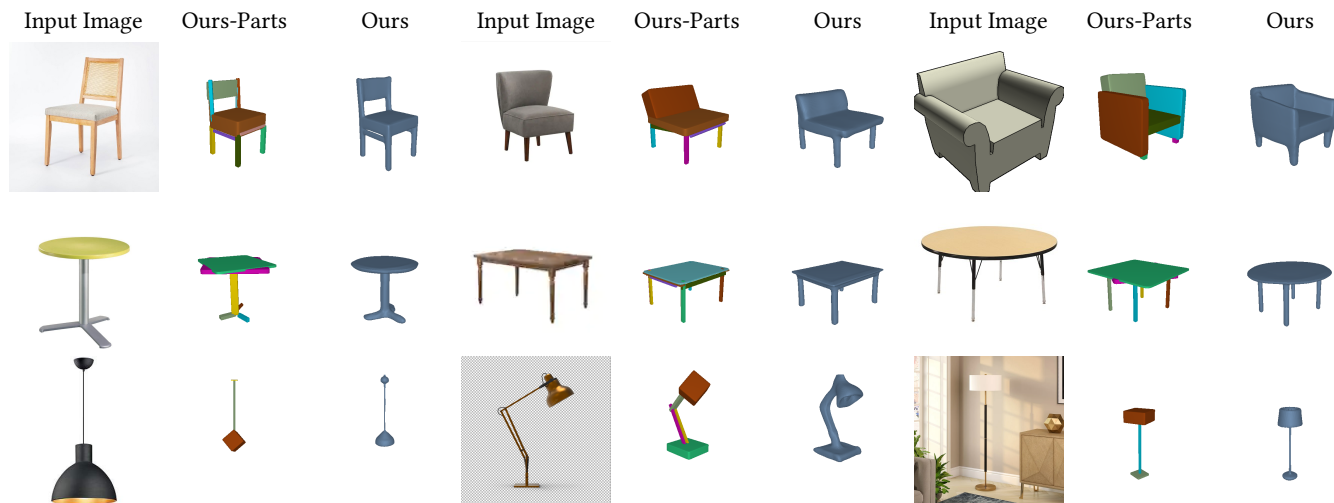


Fig. 10. **Image-guided Shape Generation.** Conditioned on various images from different object categories, our model can generate plausible 3D shapes of chairs, tables, and lamps that match the input.

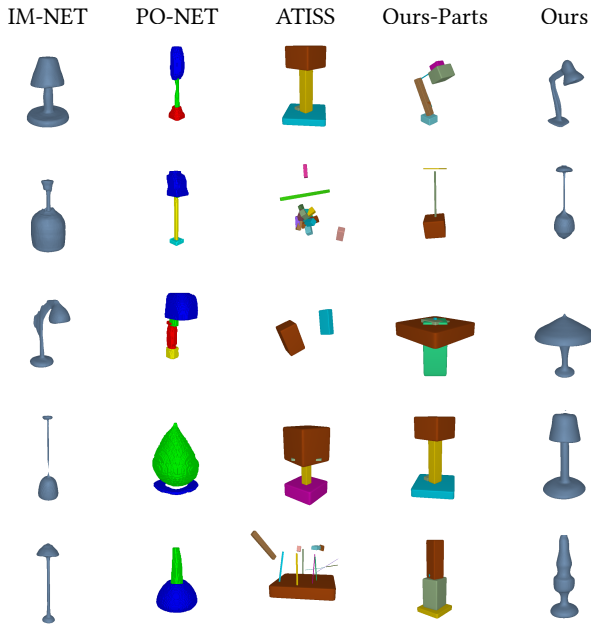


Fig. 11. **Shape Generation Results on Lamps.** We showcase randomly generated lamps using our model, ATISS, PQ-NET and IM-NET.

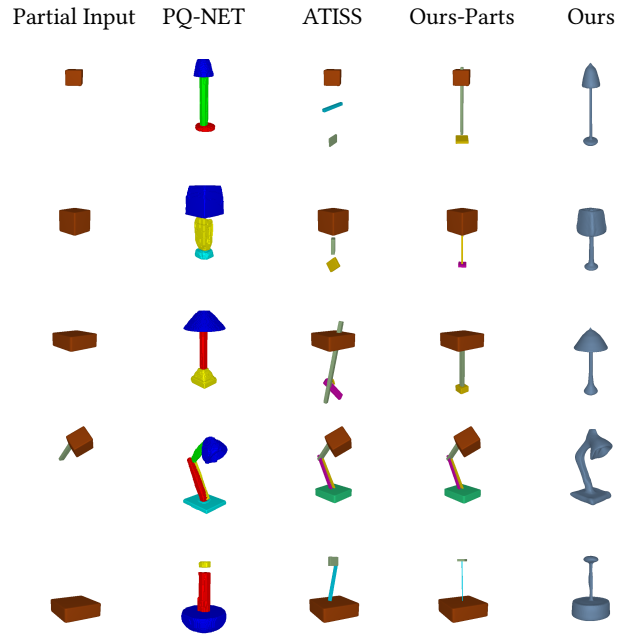


Fig. 13. **Shape Completion Results on Lamps.** Starting from partial lamps, we show completions of our model, ATISS and PQ-NET.



Fig. 12. **Shape Generation Results.** We show randomly generated chairs, tables and lamps using PASTA and our baselines, trained jointly on multiple objects categories.

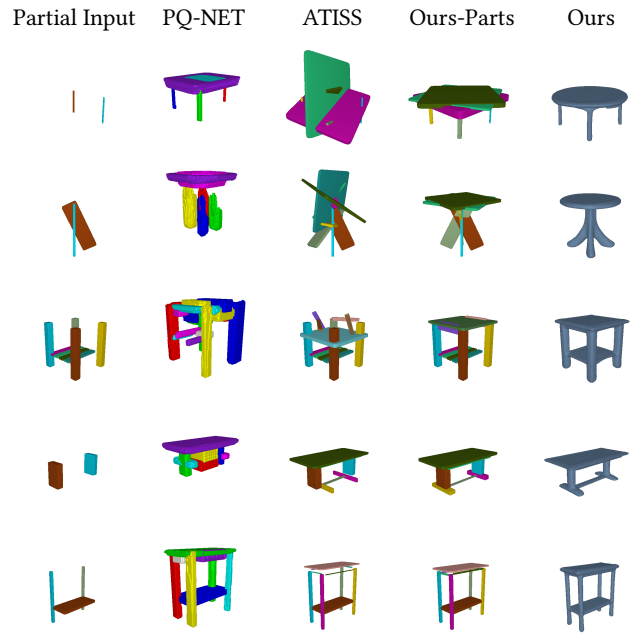


Fig. 14. **Shape Completion Results on Tables.** Starting from partial tables, we show completions of our model, ATISS and PQ-NET.

SUPPLEMENTARY MATERIAL

Abstract

In this supplementary document, we provide a detailed overview of our network architecture and the training procedure. Subsequently, we describe the preprocessing steps that we followed to filter out problematic objects from the PartNet dataset [Mo et al. 2019b]. Next, we discuss how scheduled sampling impacts the performance of our model on the scene synthesis task. Finally, we provide additional qualitative and quantitative results and analyze the limitations, future research directions, and potential negative impact of our work on society.

6 IMPLEMENTATION DETAILS

In this section, we provide a detailed description of the several components of our network architecture (Sec. 6.1). Next, we describe our training procedure (Sec. 6.2) and the generation protocol (Sec. 6.3). Finally, we detail our metrics computation (Sec. 6.4) and discuss our baselines (Sec. 6.5).

6.1 Network Architecture

Here we describe the individual components of our network architecture and provide additional implementation details. Our model comprises two main components: the *object generator* that sequentially generates objects as unordered sequences of labelled parts, where each part is parametrized using a 3D cuboidal primitive, and a *blending network* that composes part sequences in a meaningful way and synthesizes high quality implicit shapes.

Object Generator We implement our object generator using an autoregressive transformer architecture similar to ATISS [Paschalidou et al. 2021a]. In particular, it comprises three main components: (i) the *part encoder* that takes the per-part attributes and maps them to an embedding vector, (ii) the transformer encoder that takes the embeddings for each part in the sequence, the embedding of the bounding box and a learnable query embedding \mathbf{q} and predicts the feature vector \mathbf{F} and (iii) the part decoder that takes \mathbf{F} and predicts the attributes of the next object to be added in the scene.

The part encoder simply takes the attributes of each part $p_j = \{\mathbf{c}_j, \mathbf{s}_j, \mathbf{t}_j, \mathbf{o}_j\}$ and maps them to an embedding vector \mathbf{z}_j as follows:

$$\mathbf{z}_j = s_\theta \left(\left[\lambda(\mathbf{c}_j); \gamma(\mathbf{s}_j); \gamma(\mathbf{t}_j); \gamma(\mathbf{o}_j) \right] \right). \quad (6)$$

For the part label \mathbf{c}_j , we use a learnable embedding, denoted as $\lambda(\cdot)$, which is simply a matrix of size $C \times 64$, where C is the total number of part labels in the dataset. The positional encoding layer, denoted as $\gamma(\cdot)$, that is applied on the remaining attributes can be expressed as follows:

$$\gamma(p) = (\sin(2^0 \pi p), \cos(2^0 \pi p), \dots, \sin(2^{L-1} \pi p), \cos(2^{L-1} \pi p)) \quad (7)$$

where p can be any of the size, translation or rotation. We follow [Paschalidou et al. 2021a] and set $L = 32$. Once the attributes are embedded to a higher dimensional space either using $\lambda(\cdot)$ or $\gamma(\cdot)$, we concatenate them to a 512-dimensional feature vector, which is then passed to another linear layer and generates the final embedding vector $\mathbf{z}_j \in \mathbb{R}^{64}$

Similar to [Paschalidou et al. 2021a; Vaswani et al. 2017] we implement our transformer encoder as a multi-head attention transformer

without any positional encoding. Our transformer consists of 4 layers with 8 heads. The queries, keys and values have 72 dimensions and the intermediate representations for the MLPs have 1024 dimensions. We implement the transformer architecture using the transformer library provided by Katharopoulos et al. [Katharopoulos et al. 2020]¹. The learnable embedding vector \mathbf{q} and the predicted feature vector \mathbf{F} have both 64 dimensions.

The part decoder takes the feature vector \mathbf{F} as input and autoregressively predicts the attributes of the next part to be generated. The function $c_\theta(\cdot)$ that is used for the part labels is a linear layer with 64 hidden dimensions that predicts C per-label probabilities. The functions, $t_\theta^{\text{coarse}}(\cdot)$, $t_\theta^{\text{fine}}(\cdot)$, $o_\theta^{\text{coarse}}(\cdot)$, $o_\theta^{\text{fine}}(\cdot)$, $s_\theta^{\text{coarse}}(\cdot)$ and $s_\theta^{\text{fine}}(\cdot)$ are implemented using a 2-layer MLP with RELU non-linearities with hidden size 128 and output size 64. Using the $t_\theta^{\text{fine}}(\cdot)$, $o_\theta^{\text{fine}}(\cdot)$ and $s_\theta^{\text{fine}}(\cdot)$ we predict the mean, variance and mixing coefficients for the K logistic distributions for each attribute. In our experiments, we set $K = 10$.

Blending Network Our blending network consists of two main components: (i) a *part-encoder* that maps the part attributes into an embedding vector, which is implemented as discussed before and in Sec. 3.2 of our main submission and (ii) a transformer decoder without self-attention that takes the part embeddings and a set of query points and predicts their occupancy probabilities, namely whether they are inside or outside the surface boundary. We implement our transformer decoder as a multi-head cross-attention transformer without self-attention. Our transformer consists of 42 layers with 8 attention heads. The queries, keys and values have 72 dimensions and the intermediate representations for the MLPs have 1024 dimensions. To implement the transformer decoder architecture we use the transformer library provided by Katharopoulos et al. [Katharopoulos et al. 2020]².

6.2 Training Protocol

As already discussed in our main submission, we train the two components of our model independently. To train the autoregressive transformer encoder, we use the Adam optimizer [Kingma and Ba 2015] with learning rate $\eta = 10^{-4}$ and weight decay 10^{-3} . For the other hyperparameters of Adam we use the PyTorch defaults: $\beta_1 = 0.9$, $\beta_2 = 0.999$ and $\epsilon = 10^{-8}$. For both category-specific training as well as joint training experiments, we train the autoregressive transformer encoder with a batch size of 128 for 700k iterations. During training, we do not perform any type of rotation augmentation. To determine when to stop training, we follow [Paschalidou et al. 2021a] and evaluate the validation metric every 1000 iterations and use the model that performed best as our final model. Likewise, to train our blending network that is implemented using a transformer decoder we use the Adam optimizer [Kingma and Ba 2015] with learning rate $\eta = 10^{-4}$ with no weight decay. For the other hyperparameters of Adam we use the PyTorch defaults: $\beta_1 = 0.9$, $\beta_2 = 0.999$ and $\epsilon = 10^{-8}$. For the case of category-specific training, we train the transformer on each object category with a batch size of 32 for 150k iterations. For the case of the joint-training on multiple object categories, we train the blending network with a batch size of 32 for

¹<https://github.com/idiap/fast-transformers>

²<https://github.com/idiap/fast-transformers>

300k iterations. To train the blending network, we need to generate occupancy pairs, namely points accompanied by a label indicating whether this point lies inside or outside the target mesh. To this end, we sample 180,000 points uniformly in a cube ranging from -1 to 1 centered at (0, 0, 0) plus 20,000 points from the surface for each mesh and compute which of these points lie inside or outside the mesh. During training, we sample 2048 occupancy pairs from an unbalanced distribution that, in expectation, results in an equal number of points with positive and negative labels. Note that we follow common practice and compute importance sampling weights in order to reweigh our loss and create an unbiased estimator of the loss with uniform sampling similar to [Paschalidou et al. 2019]. All our experiments were conducted on a single NVIDIA 2080 Ti GPU, with 11GB of memory, and training of both components of our architecture takes approximately 2 days.

6.3 Generation Protocol

In this section, we discuss the sampling process for generating a novel part arrangement. When we perform generation from scratch, we condition our generation on a bounding box that specifies the object boundaries. Note that when we want to generate novel shapes from a model that was trained jointly on multiple object categories, we do not have to explicit condition on a specific category. For the case of shape completion from an incomplete sequence of parts, we condition our generation on the cuboidal primitives as well as the bounding box that specifies the object boundaries. A similar concept is adapted for the case of the language- and image-guided generation. As soon as a sequence of cuboidal parts is produced, we pass it to the transformer decoder that composes the cuboids and synthesizes an implicit 3D shape of high quality.

6.4 Metrics

As mentioned in the main submission, to evaluate the plausibility and the diversity of the generated shapes using our model and our baselines, we report the Coverage Score (COV) and the Minimum Matching Distance (MMD) [Achlioptas et al. 2018] using the Chamfer- L_2 distance between points sampled on the surface of the real and the generated shapes. In particular, MMD measures the *quality of the generated shapes* by computing how likely it is that a generated shape looks like a shape from the reference set of shapes. On the other hand, COV measures how many shape variations are covered by the generated shapes, by computing the percentage of reference shapes that are closest to at least one generated shape.

Let us denote G the set of generated shapes and R the set of reference shapes from the test set. To estimate the similarity between two shapes from the two sets, we use the Chamfer Distance (CD), which is simply the distance between a set of points sampled on the surface of the reference and the generated mesh. Namely, given a set of N sampled points on the surface of the reference $\mathcal{X} = \{\mathbf{x}_i\}_{i=1}^N$ and the generated shape $\mathcal{Y} = \{\mathbf{y}_i\}_{i=1}^N$ the Chamfer Distance (CD) becomes

$$\text{CD}(\mathcal{X}, \mathcal{Y}) = \frac{1}{N} \sum_{\mathbf{x} \in \mathcal{X}} \min_{\mathbf{y} \in \mathcal{Y}} \|\mathbf{x} - \mathbf{y}\|_2^2 + \frac{1}{M} \sum_{\mathbf{y} \in \mathcal{Y}} \min_{\mathbf{x} \in \mathcal{X}} \|\mathbf{y} - \mathbf{x}\|_2^2. \quad (8)$$

In all our evaluations, we set $N = 2048$. Note that to compute the Chamfer distance between our generated part-based representations and real objects from the test set, we sample points on the surface of the union of the generated cuboids and compute their distance to points sampled from the reference shapes.

The Minimum Matching Distance (MMD) is the average distance between each shape from the generated set G to its closest shape in the reference set R and can be defined as:

$$\text{MMD}(G, R) = \frac{1}{|R|} \sum_{\mathcal{X} \in R} \min_{\mathcal{Y} \in G} \text{CD}(\mathcal{X}, \mathcal{Y}). \quad (9)$$

Intuitively, MMD measures how likely it is that a generated shape is similar to a reference shape in terms of Chamfer Distance and is a metric of the plausibility of the generated shapes. Namely, a high MMD score indicates that the shapes in the generated set G faithfully represent the shapes in the reference set R .

The Coverage score (COV) measures the percentage of shapes in the reference set that are closest to each shape from the generated set. In particular, for each shape in the generated set G , we assign its closest shape from the reference set R . In our measurement, we only consider shapes from R that are closest to at least one shape in G . Formally, COV is defined as

$$\text{COV}(G, R) = \frac{|\{\text{argmin}_{\mathcal{X} \in R} \text{CD}(\mathcal{X}, \mathcal{Y}) \mid \mathcal{Y} \in G\}|}{|G|} \quad (10)$$

Intuitively, COV measures the diversity of the generated shapes in comparison to the reference set. In other words, a high Coverage indicates that most of the shapes in the reference set R are roughly represented by the set of generated shapes G . To ensure a fair comparison with our baselines, we generate 2000 shapes per object category for each baseline and compare it with 225, 1216, 1477 test shapes from the lamps, chairs and tables categories respectively. Note that both the generated and the target shapes from the test set are scaled within the unit cube before the metrics computations.

6.5 Baselines

In this section, we provide additional details regarding our baselines. We compare our model with IM-NET [Chen and Zhang 2019], PQ-NET [Wu et al. 2020] and ATISS [Paschalidou et al. 2021a]. For all our experiments, we retrain all baselines, using the released code provided by the authors. For the case of ATISS, which is an autoregressive transformer originally introduced for indoor scene synthesis, we adapt the original code³ for the task of part-based object generation and train ATISS using the per-object part sequences from PartNet [Mo et al. 2019b]. Note that IM-NET [Chen and Zhang 2019] is not directly comparable to our model as it does not consider any parts. However, we include it in our evaluation as a powerful implicit-based generative model for 3D shapes.

IM-NET: IM-NET [Chen and Zhang 2019] was among the first methods that proposed to implicitly represent 3D object geometries in the weights of a neural network. In particular, given an input feature representation and a 3D point, their model predicts whether the query 3D point lies inside or outside the object’s surface boundaries. IM-NET can be combined with several generative frameworks such

³<https://github.com/nv-tlabs/ATISS>

as Variational Autoencoders (VAEs) [Kingma and Welling 2014] or Generative Adversarial Networks (GANs) [Goodfellow et al. 2014]. In our experiments, we consider the latter, referred to as IM-GAN in the original paper, that utilizes a latent GAN [Achlioptas et al. 2018] directly trained on the latent feature space of a voxel-based autoencoder. Note that IM-GAN relies on two-stage training, namely, first train the autoencoder and then train the GAN on the autoencoder’s latent space. In our experiments, we train IM-NET using their Tensorflow implementation [Abadi 2016]⁴ with the default parameters until convergence, on the preprocessed data released by the authors. Training of both the autoencoder and the latent GAN took approximately 2 days on a single NVIDIA 2080 Ti GPU.

PQ-NET: In PQ-NET [Wu et al. 2020], the authors introduce a generative model that synthesizes 3D shapes sequentially using a set of parts parametrized as volumetric Signed Distance Fields (SDFs). In detail, PQ-NET comprises three core components that need to be trained sequentially. First, the *part autoencoder* learns a mapping between the voxelized part-based representation of a 3D shape to a volumetric SDF. Next, a sequence-to-sequence autoencoder, implemented with two RNNs [Schuster and Paliwal 1997] is employed, which takes as input a sequence of per-part features and maps them to a latent feature representation that describes the assembled 3D shape. This representation is then passed to a sequential decoder that predicts a sequence of meaningful parts. Lastly, to generate novel 3D shapes, a GAN [Achlioptas et al. 2018] is trained on the latent space of the sequential autoencoder. We train PQ-NET using the provided PyTorch [Paszke et al. 2016]⁵ implementation with the default parameters until convergence. Note that in our experiments, we do not exclude shapes with more than 10 shapes from our training data, as in the original paper. Instead, we consider chairs and tables with at most 50, and lamps with no more than 30 parts. Unlike our model, considering shapes with a larger number of parts is not possible, because it results in excessive memory usage that prevents training PQ-NET’s seq2seq module on a single GPU. Specifically, PQ-NET’s part auto-encoder requires 3 NVIDIA 2080 Ti GPU. Part seq2seq module and GAN require 1 NVIDIA 2080 Ti. The training of all three components took approximately 4-5 days.

ATISS: In ATISS [Paschalidou et al. 2021a], the authors introduce an autoregressive transformer architecture for indoor scene synthesis. In our experiments, we repurpose the original PyTorch [Paszke et al. 2016]⁶ implementation in order to be able to utilize it for the object generation task. In particular, each object is represented as a collection of labelled cuboidal primitives and we train ATISS to maximize the log-likelihood of all possible permutations of part arrangements in a collection of training data. We train ATISS using the default parameters for 1200 epochs on an NVIDIA 2080 Ti GPU for approximately 1-2 days, without any data augmentation. Unlike PQ-NET, to train ATISS, we do not filter out shapes with a larger number of parts. Specifically, we consider the same set of shapes used to train our model, namely chairs, tables and lamps with a maximum number of 144, 164, 191 parts respectively.

⁴<https://github.com/czq142857/IM-NET>

⁵<https://github.com/ChrisWu1997/PQ-NET>

⁶<https://github.com/nv-tlabs/ATISS>

6.6 Mesh Extraction

To extract meshes from the predicted occupancy field, we employ the Marching Cubes algorithm [Lorensen and Cline 1987]. In particular, we start from a voxel grid of 128^3 initial resolution for which we predict occupancy values. Next, we follow the process proposed in [Mescheder et al. 2019] and extract the approximate isosurface with Marching Cubes using the code provided by Mescheder et al. [Mescheder et al. 2019]. Note that the same process is followed to extract meshes from the implicit representations learned both with PQ-NET [Wu et al. 2020] and IM-NET [Chen and Zhang 2019].

7 DATA PROCESSING

We use PartNet [Mo et al. 2019a] as the dataset to evaluate our model and our baselines. We remove 123 objects in total across all categories due to their invalid part hierarchical structures (i.e. missing nodes etc.). To train our blending network, we assume explicit 3D supervision in the form of a watertight mesh. To acquire this, we align ShapeNet [Chang et al. 2015] objects with PartNet objects using the scripts provided in the official PartNet repository⁷. We then convert aligned objects into watertight meshes using the code provided by Stutz et al. [Stutz and Geiger 2018]⁸. To train the variant of our model for language-guided generation, we remove samples, whose descriptions are too long and cannot be handled by CLIP [Radford et al. 2021]. After this processing step, we have 4000 training samples for chairs, 5439 for tables, and 1424 for lamps.

Fig. 15 visualizes the part sequences for all object categories. We note that chairs contain more samples with longer sequences, while lamps tend to have objects with fewer components, hence making them easier to generate.

8 IMPACT OF SCHEDULE SAMPLING

In this section, we investigate how schedule sampling affects the generation capabilities of our model. For this experiment, we perform category specific training on the Chair category. In particular, we train two variants of our model, one with teacher forcing and one with schedule sampling until convergence. We compare the two model variants wrt. their generation performance in Tab. 3. We note that training our network only with teacher forcing, significantly deteriorates performance and results in generations of lower quality. This is also validated from our qualitative compari-

| | MMD-CD (↓) | COV-CD (% ↑) |
|----------------------------|-------------|--------------|
| Ours w/o Schedule Sampling | 3.74 | 56.99 |
| Ours | 3.21 | 57.73 |

Table 3. **Ablation Study on Schedule Sampling.** This table shows a quantitative comparison of our approach trained with teacher forcing and our proposed schedule sampling strategy. We compare the two variants of our model wrt. the MMD-CD (↓) and the COV-CD (↑) between generated and real shapes from the test set.

son in Fig. 16, where we visualize randomly generated chairs using both models. We observe that the variant of our model trained only with teacher forcing tends to produce part arrangements, with parts

⁷<https://partnet.cs.stanford.edu/>

⁸https://github.com/paschalidou/mesh_fusion_simple

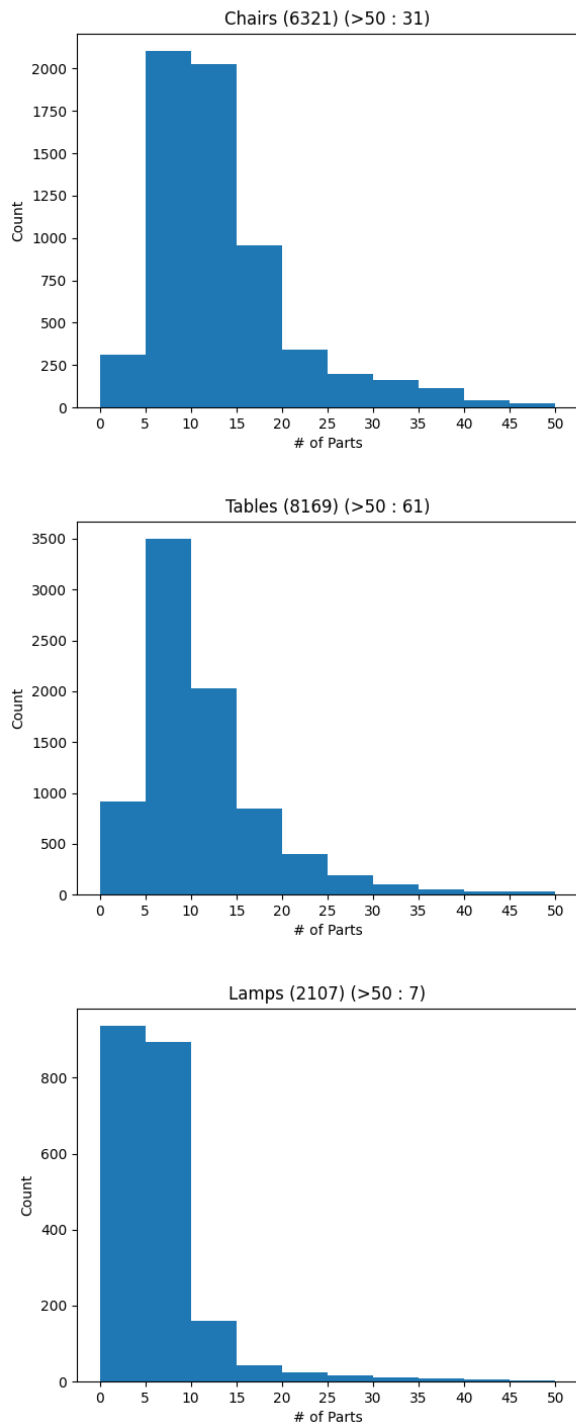


Fig. 15. Sequence Lengths of all Object Categories.

placed in unnatural positions. On the contrary, when training our model with our proposed schedule sampling strategy, we observe

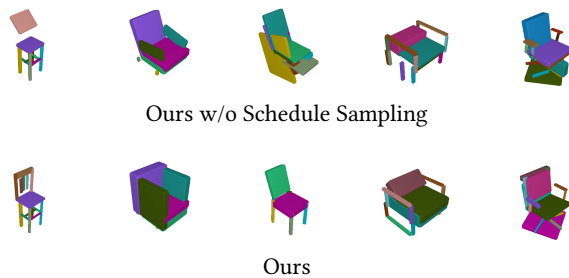


Fig. 16. **Impact of Schedule Sampling.** We show randomly generated samples of our model trained with teacher forcing (first row) and compare with randomly generated samples of our model trained with our schedule sampling strategy (second row).



Fig. 17. **Example Rendering of Target Images for FID Computation.**

that our model consistently generate plausible part sequences. This is expected as schedule sampling allows training our model with imperfect data, which makes it more robust to imperfect generations. Namely, even if one of the generated parts is problematic, our network can produce plausible parts in the next generation steps.

9 ADDITIONAL EXPERIMENTAL RESULTS

In this section, we provide additional information regarding our experiments on PartNet [Mo et al. 2019b]. In particular, we consider three categories: *Chair*, *Table* and *Lamp*, which contain 4489, 5705, and 1554 shapes respectively. For the *Chair* category, there are 47 different classes (e.g. back surface horizontal bar, arm holistic frame etc.) in total, while for the *Lamp* and *Table*, we have 32 and 43 part categories respectively. Note that unlike prior works such as PQ-NET [Wu et al. 2020] that only consider shapes that have less than 10 parts, we consider shapes with a significantly larger number of components. In particular, chairs can have up to 144 parts, tables 164 parts and lamps up to 191 parts. For more details, regarding our training data, we refer reader to Sec. 7. In this section, we provide additional qualitative results for all experiments discussed in our main submission.

9.1 Shape Generation

In this experiment, we investigate the ability of our model to generate plausible part-aware 3D geometries, conditioned on various bounding boxes that specify the object’s boundaries. Fig. 18 shows seven randomly generated chairs using our model, ATISS [Paschalidou et al. 2021a], PQ-NET [Wu et al. 2020] and IM-NET [Chen and Zhang 2019]. Note that for this experiment, we perform category-specific training, namely we train a different model for each object type. For our model, we visualize both the synthesized part arrangements (Ours-Parts) and the output of our blending network

| | MMD-CD (\downarrow) | | | COV-CD ($\%, \uparrow$) | | | FID (\downarrow) | | | Classification Accuracy | | |
|------------|-------------------------|-------------|-------------|---------------------------|--------------|--------------|----------------------|-------------|-------------|------------------------------------|-----------------------------------|-------------------------------------|
| | Chair | Table | Lamp | Chair | Table | Lamp | Chair | Table | Lamp | Chair | Table | Lamp |
| PQ-Net | 4.69 | 3.64 | 4.55 | 35.77 | 42.31 | 53.33 | - | - | - | - | - | - |
| ATISS | 4.33 | 3.40 | 5.90 | 44.57 | 43.33 | 60.88 | 13.63 | 30.87 | 25.86 | 76.85 ± 1.8 | 72.16 ± 1.2 | 45.7 ± 9.84 |
| Ours-Parts | 3.43 | 2.66 | 5.72 | 50.49 | 56.13 | 57.78 | 3.92 | 3.90 | 15.2 | 60.83 ± 0.59 | 65.9 ± 0.01 | 48.55 ± 10.16 |
| Ours | 3.11 | 2.33 | 5.58 | 49.00 | 58.56 | 51.00 | - | - | - | - | - | - |

Table 4. **Shape Completion.** We measure the MMD-CD (\downarrow), the COV-CD (\uparrow), the FID score (\downarrow) and the Parts Classification Accuracy between the part-based representations of completed and real shapes from the test set. Classification accuracy closer to 0.5 is better.

that composes the sequence of the generated cuboids into a single high-quality implicit shape. We observe that our synthesized part sequences are consistently meaningful. For the case of ATISS, we note that the generated cuboids are placed in unnatural positions, hence producing non-functional objects. We hypothesize that this is mainly due to the large number of parts that typically compose chairs. On the contrary, we observe that both PQ-NET and IM-NET produce plausible chairs. For the case of tables (see Fig. 19), we observe that our model consistently generates meaningful part sequences, whereas ATISS again produces part arrangements, where parts are placed in unnatural positions. For PQ-NET, we observe that in some cases, it tends to generate non-functional tables with less legs (see 5th row in Fig. 19). Finally, we also provide seven generated lamps of our model and our baselines in Fig. 20. For the case of lamps, both our model and ATISS seem to be able to generate realistic sequences of cuboids. For all the experiments in this section, as well as the results in Sec. 4.1 of our main submission we condition the generation on randomly sampled bounding boxes from the test set.

For all object categories, we observe that our blending network composes the generated part sequences in a meaningful way and synthesizes novel 3D shapes that respect the provided part-based structure. The output representation of our blending network is of higher quality than IM-NET [Chen and Zhang 2019] that also generates implicit 3D shapes, as indicated by our quantitative evaluation from Table 1 in our main submission.

9.2 Shape Completion

Starting from a partial object, parameterized with a set of cuboidal parts, we want to evaluate whether our model and our baselines can generate plausible part arrangements. Since IM-NET cannot be used to complete 3D shapes from a partial sequence of parts, we exclude it from our evaluation. To measure the quality of the generated parts, in this experiment, we also report the classification accuracy of a classifier trained to discriminate real from synthetic objects. In particular, as we represent objects using a collection of cuboidal primitives, we implement our classifier using a transformer encoder [Vaswani et al. 2017] trained to discriminate real from generated 3D labelled cuboids. Furthermore, in our evaluation, we also the FID score [Heusel et al. 2017]. For the FID score computation, we generate the same amount of objects as in the test set and render them at 512×512 resolution using 5 random camera views. To evaluate the realism of the generated parts, we render objects using their part-based representation, as show in Fig. 17, and we compare with corresponding part-based renderings from the ground-truth objects

from the test set, rendered using the same camera distribution. We follow common practice and repeat the metric computation for FID 10 times and report the mean. The quantitative results for this experiment are summarized in Tab. 4. Note that we compare our model only two ATISS wrt. FID and classification accuracy, which also generates objects as a sequence of cuboidal primitives.

To generate the partial objects, we randomly sample objects from the test set and generate the partial input by removing an arbitrary set of parts. As mentioned also in our main submission, to ensure a fair comparison to PQ-NET, for this task instead of conditioning on the partial set of cuboids, we utilize the corresponding 3D parts that were used during the PQ-NET’s training. The 1st column in Fig. 22, Fig. 23 and Fig. 24 shows the partial input in the form of 3D cuboids that is used in the case of PASTA and ATISS. For PQ-NET, we utilize the actual 3D parts that correspond to each cuboid. Both from the quantitative analysis in Tab. 4, as well as the qualitative results in Fig. 22 and Fig. 23, we observe that our model completes the partial input chairs and table in a more plausible way, than both PQ-NET and ATISS. Note that, since PQ-NET employs a sequence-to-sequence autoencoder to generate part sequences, there is no guarantee that the original part sequence, will also appear in the completed sequence. For the case of ATISS, we observe that it struggles completing the partial input in a meaningful way. For example, the added parts are placed in non realistic positions (see last row in Fig. 22 and 3rd row in Fig. 23. For the case of lamps, we note that all three models can successfully complete the partial sequence.

9.3 Size-guided Generation

Now we examine whether our model can generate objects of different sizes. Note that as we condition the generation of parts on a bounding box that defines the object boundaries, our model can generate shapes of arbitrary sizes. In this experiment, we generate several bounding boxes, with different size parameters and demonstrate the ability of our model to generate short and tall lamps (see 1st and 3rd lamp in 3rd row in Fig. 21, respectively), or smaller and bigger tables (see 1st and 2nd tables in 2nd row in Fig. 21). We believe that this is an important application of our model that allows users to precisely specify the size of the generated object. For all experiments presented in Fig. 21, we perform category-specific training per object type.

9.4 Language-guided Generation

Starting from a text prompt and a bounding box that defines the object’s boundaries, we want to examine the ability of our model



Fig. 18. **Shape Generation Results on Chairs.** We show randomly generated chairs using our model, ATISS [Paschalidou et al. 2021a], PQ-NET [Wu et al. 2020] and IM-NET [Chen and Zhang 2019].



Fig. 19. **Shape Generation Results on Tables.** We showcase randomly generated tables using our model, ATISS [Paschalidou et al. 2021a], PQ-NET [Wu et al. 2020] and IM-NET [Chen and Zhang 2019].



Fig. 20. **Shape Generation Results on Lamps.** We showcase randomly generated lamps using our model, ATISS [Paschalidou et al. 2021a], PQ-NET [Wu et al. 2020] and IM-NET [Chen and Zhang 2019].



Fig. 21. **Size-guided Shape Generation.** Conditioned on bounding boxes of different sizes, our model can generate shapes that match the conditioning..

to generate plausible part arrangements that match the input text descriptions. To this end, for this task, we utilize the part labels provided in PartNet [Mo et al. 2019b] and generate text descriptions that describe the part-based structure for each object. Some examples of the produced text descriptions for various object categories are summarized below:

- A chair with four leg, one bar stretcher, three runners, one seat single surface, one arm horizontal bar, two arm near vertical bars, two arm horizontal bars, two arm near vertical bars, one arm horizontal bar, and one back single surface.
- A chair with four leg with two runners, one seat single surface, and one back single surface.
- A table with one drawer front, one handle, one drawer front, one handle, two vertical side panels, one bottom panel, four leg, one back panel, one vertical front panel, and one board.
- A table with one central support, one pedestal, one tabletop connector, one other, one board, and one tabletop frame.
- A lamp with one lamp shade, one light bulb, one other, one chain, and one lamp base part.
- A lamp with one lamp arm straight bar, one lamp shade, one light bulb, one other, one lamp base part, and one lamp body.

Using these text descriptions, we utilize a pre-trained CLIP [Radford et al. 2021]⁹ text encoder to extract embeddings for the shape’s textual descriptions. During training, we condition our generation both on the CLIP text embeddings and the embedding produced from the bounding box, containing the object. Note that during training the CLIP text-encoder is not optimized with the rest of our architecture. While our model was not trained with free-text descriptions, we showcase that by exploiting CLIP’s powerful latent space our model can generate plausible part arrangements and 3D objects that match the input text prompt (see Fig. 25). To be able to control the shape of the generated shape e.g. generate a small chair or a narrow table, it simply suffices to condition the generation on a bounding box that fits these criteria. For now, we do this manually, namely we generate a bounding box that fits the text input.

⁹<https://github.com/OpenAI/CLIP>

9.5 Image-guided Generation

For this task, we utilize the variant of our model that was trained for language-guided generation without any re-training. CLIP [Radford et al. 2021] learns a common latent space between images and sentences that describe them. Therefore, we take advantage of CLIP’s joint latent space, and use the variant of our model trained for language-guided generation, to synthesize plausible 3D shapes from images, simply by replacing the CLIP’s text encoder, with the corresponding CLIP image encoder. While our model was only trained with text embeddings, we showcase that it can successfully generate part sequences that match the input image (see Fig. 26). Note that the recovered parts capture fine geometric details such as the circular base of the 2nd chair, in the second row in the Fig. 26, and our model is able to generate realistic shapes conditioned on images with and without backgrounds.

9.6 Generating Part Variations

Finally, we also demonstrate that our model can produce plausible part variations for a specific part, selected by the user. For example in Fig. 27, we select the back of the chair, highlighted with red and show that our model can generate variations of the selected part with different sizes.

10 DISCUSSION AND LIMITATIONS

In this work, we devise PASTA, a part-aware generative model for 3D shapes. Our architecture, consists of two main components: the *object generator* that autoregressively generates objects as sequences of labelled cuboids and the *blending network* that composes a sequence of cuboidal primitives and synthesizes a high-quality implicit shape. We train the object generator to maximize the log-likelihood of all part arrangements, in the dataset. Unlike prior part-based works [Wu et al. 2020], our model is simpler to train and only requires part annotations in the form of cuboids and not the actual parts, which are typically harder to acquire. Moreover, our blending network, which is implemented with a transformer decoder, generates 3D shapes of high fidelity from the sequence of the generated cuboids. The supervision for training our blending network comes in the form of watertight meshes. From our experimental evaluation it becomes evident that our model outperforms existing part-based and non-part based methods both on the task of shape generation and completion. Furthermore, we showcase several applications of our model, such as language- and image-guided shape generation.

Although, we believe that our model is an important step towards automating 3D content creation, it has several limitations. Firstly, our model requires part-supervision, which is difficult to acquire, thus hindering applying our model to other data. Recent works [Hao et al. 2020; Hertz et al. 2022] proposed generative models that can be trained without part-level annotations but as they are not autoregressive they cannot be used for several completion tasks. We believe that an exciting direction for future research is to explore whether we can learn an autoregressive generative model of parts, without explicit part-level supervision. Note that this task is not trivial, since training autoregressive models with teacher forcing or schedule sampling requires part annotations. Furthermore, while our model can generate plausible 3D geometries, in this work, we

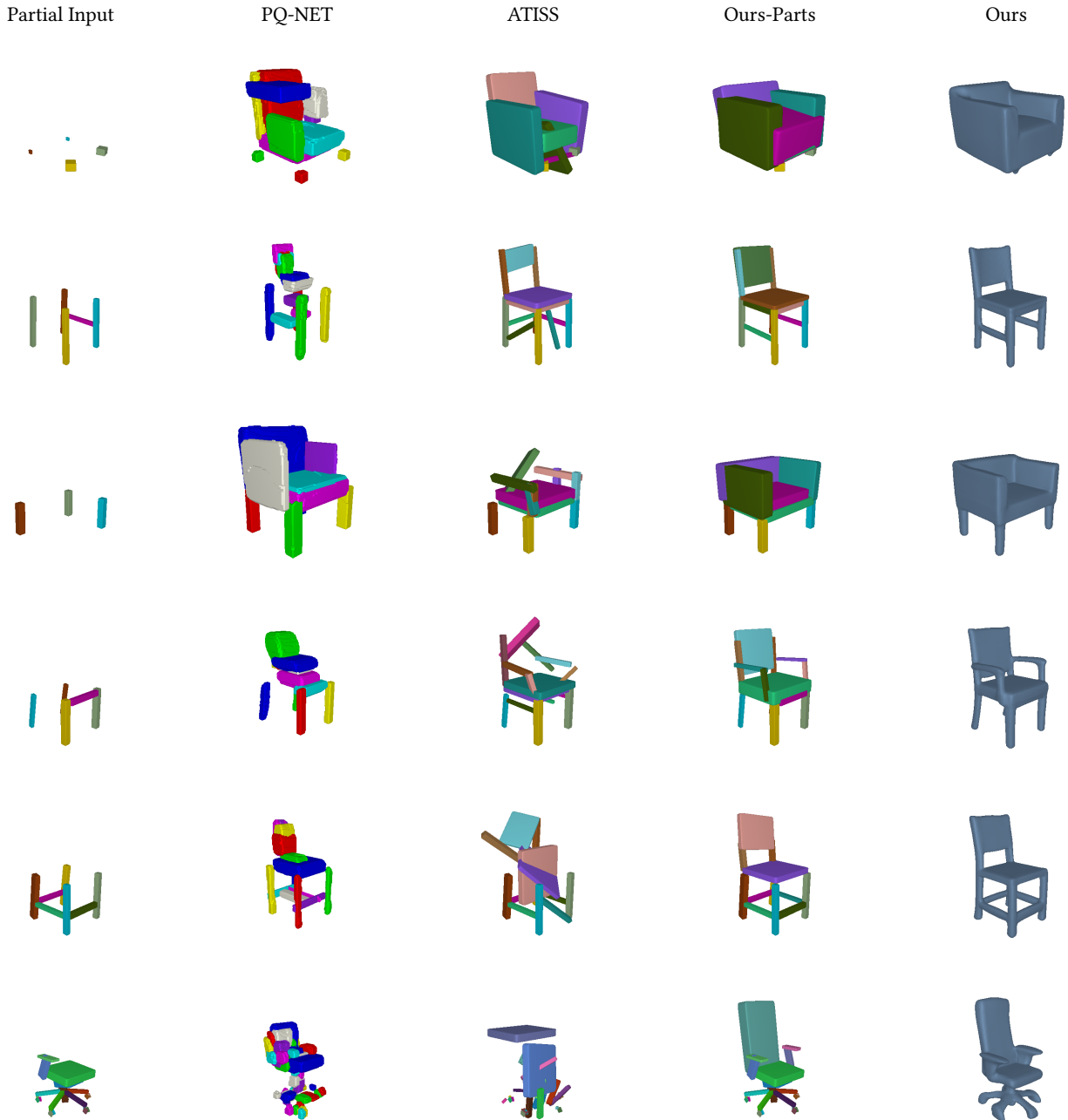


Fig. 22. **Shape Completion Results on Chairs.** Starting from partial chairs, we show completions of our model, ATISS [Paschalidou et al. 2021a] and PQ-NET [Wu et al. 2020].

do not consider the object’s appearance. We believe that another interesting direction for future research would be to explore learning a generative model of parts with textures. This would unlock more editing operations both on the object’s geometry and appearance. In our current setup, this can be easily done, simply by replacing our blending network with a NeRF-based decoder [Mildenhall et al.

2020] that instead of only predicting occupancies, predicts colors and opacity values for the set of query points.

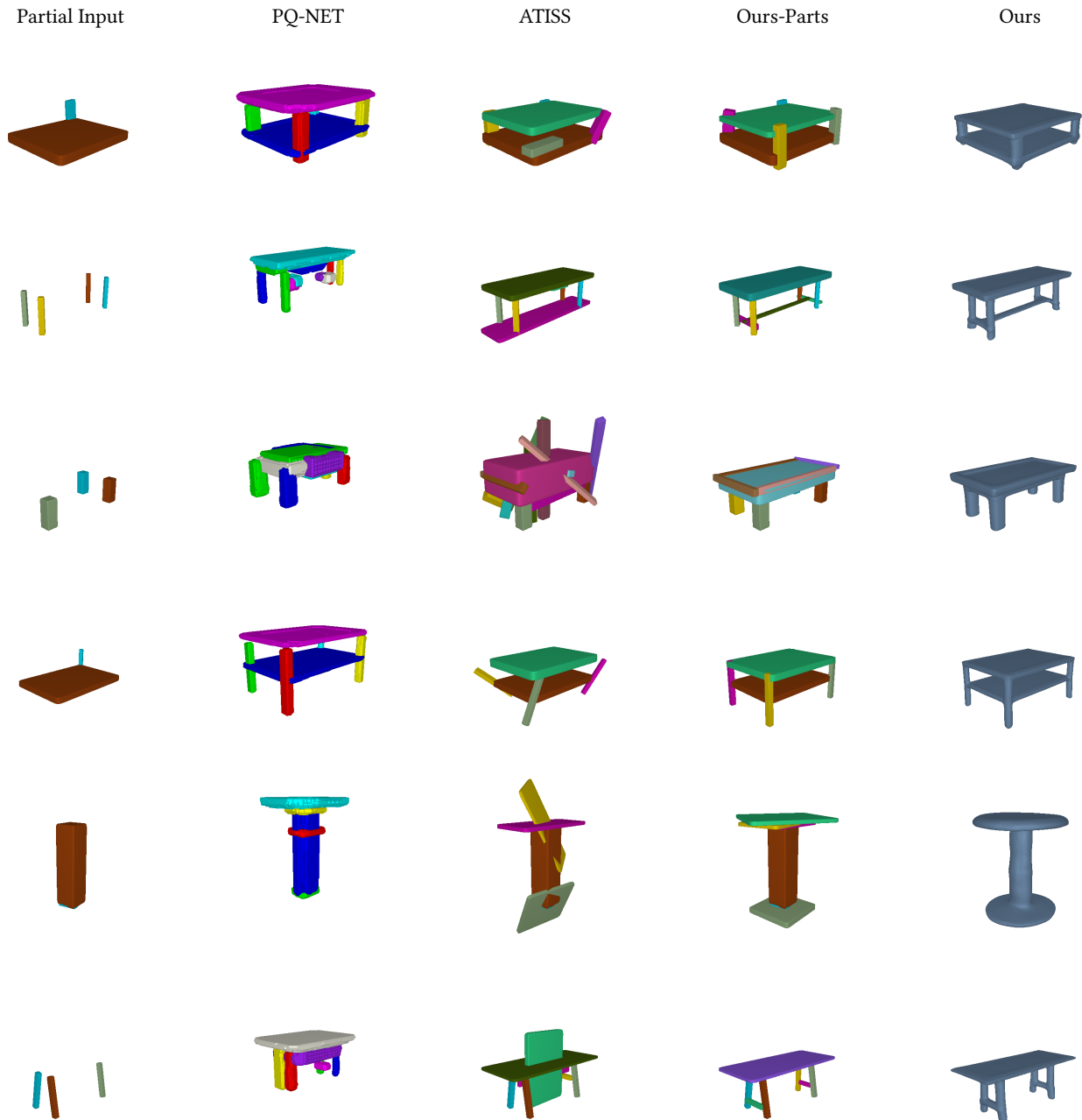


Fig. 23. **Shape Completion Results on Tables.** Starting from partial tables, we show completions of our model, ATISS [Paschalidou et al. 2021a] and PQ-Net [Wu et al. 2020].

11 POTENTIAL NEGATIVE IMPACT ON SOCIETY

Our proposed model enables generating part-aware 3D shapes as well as several editing operations such as size-, image- and language-guided generation. While, we see our work as an important step towards automatic content creation and enabling a multitude of editing functionalities, it can also lead to negative consequences,

when applied to sensitive data, such as human bodies. Therefore, we believe it is imperative to always check the license of any publicly available 3D model. In addition, we see the development of techniques for identifying real from synthetic data as an essential research direction that could potential prevent deep fake. While throughout this work, we have only worked with publicly available

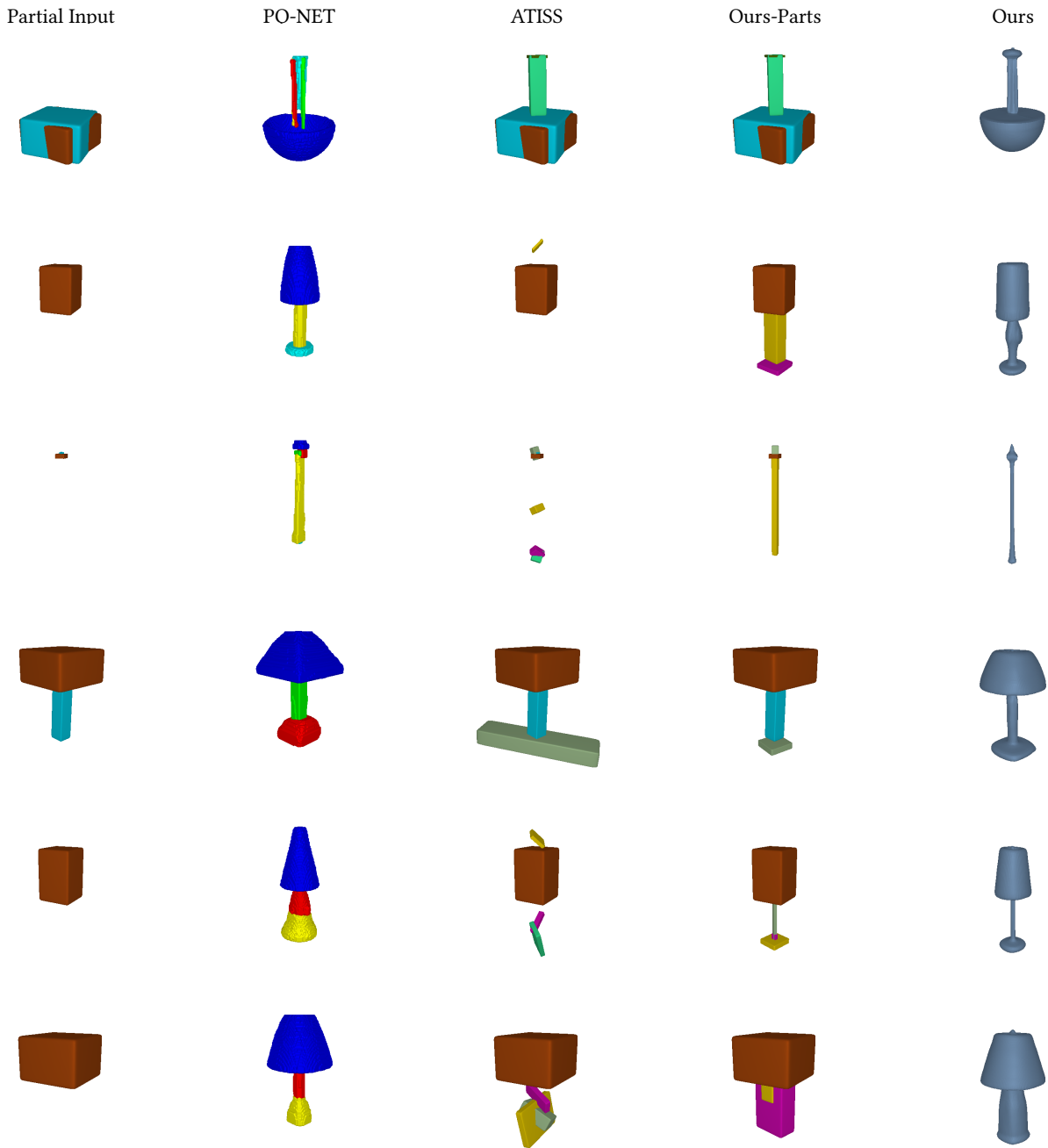


Fig. 24. **Shape Completion Results on Lamps.** Starting from partial lamps, we show completions of our model, ATISS [Paschalidou et al. 2021a] and PQ-NET [Wu et al. 2020].

datasets, we recommend that future users that will train our model on new data to remove biases from the training data in order to

ensure that our model can fairly capture the diversities in terms of shapes and sizes.



Fig. 25. **Text-guided Shape Generation.** Given different text descriptions our model can generate plausible 3D shapes of chairs, tables, and lamps.

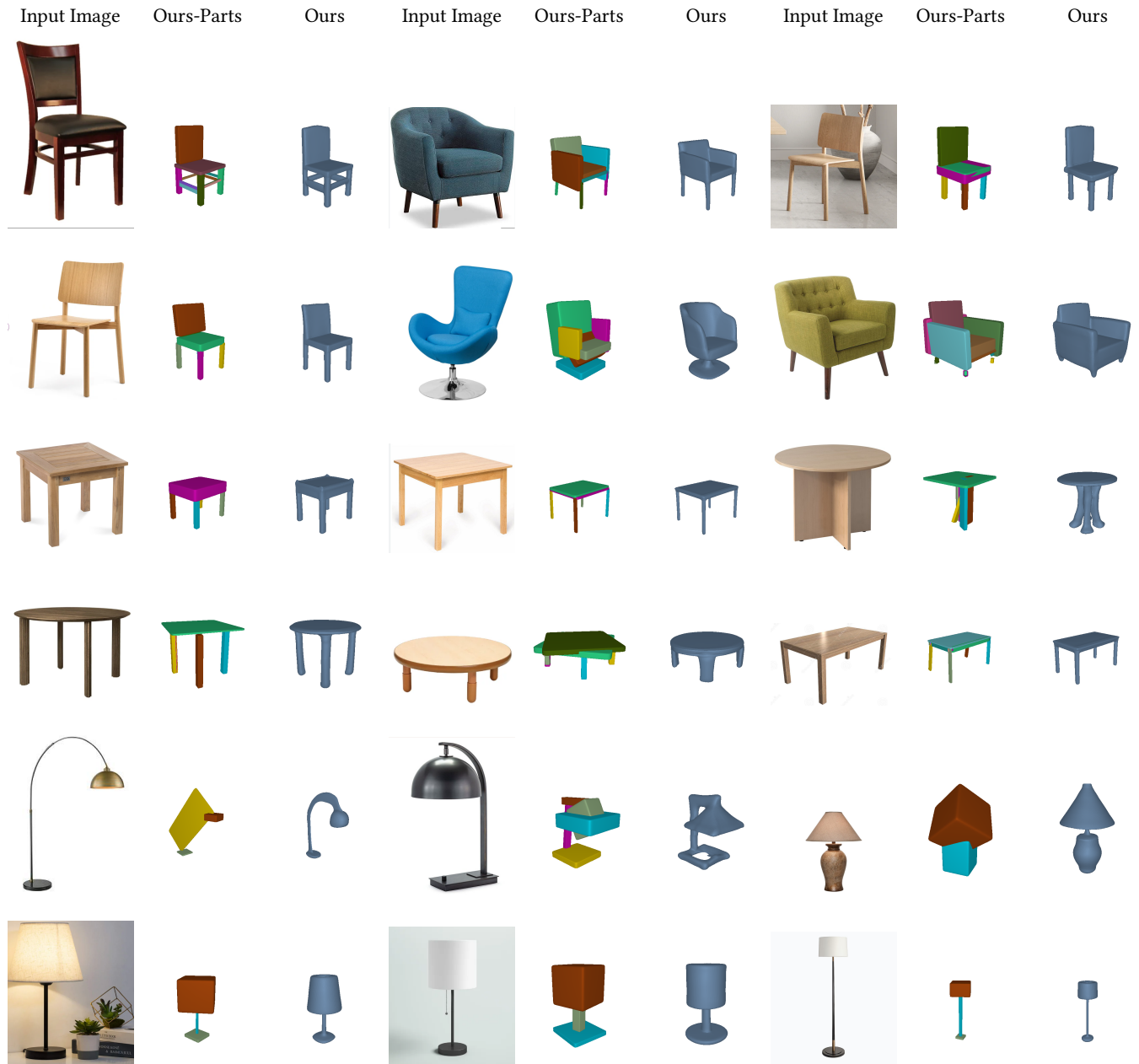


Fig. 26. **Image-guided Shape Generation.** Given different images our model can generate plausible 3D shapes of chairs, tables, and lamps. Note that for this experiment, we employ the variant of our model trained for language-guided training, without any re-training.

Input Shape

Variation 1

Variation 2

Variation 3

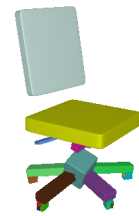
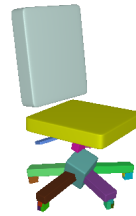
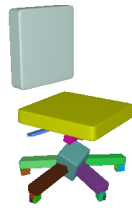


Fig. 27. **Generating Part Variations** For the same part, highlighted with red, we showcase that our network can generate plausible part variations.